Chapter 2
Climate Dynamics

The most noticeable facets of the weather are those which directly impinge on us: wind, rain, sun, snow. It is hotter at the equator than at the poles simply because the local intensity of incoming solar radiation is greater there, and this differential heating drives (or tries to), through its effect on the density of air, a poleward convective motion of the atmosphere: rising in the tropics, poleward in the upper atmosphere, down at the poles and towards the equator at the sea surface. The buoyancy-induced drift is whipped by the rapid rotation of the Earth into a predominantly *zonal flow*, from west to east in mid-latitudes. In turn, these zonal flows are *baroclinically* unstable, and form waves (Rossby waves) whose form is indicated by the isobar patterns in weather charts.[1]

All this frenetic activity obscures the fact that the weather is a rather small detail in the determination of the basic climate of the planet. The mean temperature of the planetary atmosphere and of the Earth's surface is determined by a balance between the radiation received by the Earth from the Sun (the incoming solar radiation), and that re-emitted into space by the Earth.

2.1 Radiation Budget

We denote the incoming solar radiation by Q; it has a value $Q = 1370\ \mathrm{W\,m^{-2}}$ (watts per square metre). A fraction a of this (the albedo) is reflected back into space, while the rest is absorbed by the Earth; for the Earth, $a \approx 0.3$. In physics we learn that a perfect radiative emitter (a *black body*) at absolute surface temperature T emits energy at a rate

$$E_b = \sigma T^4, \tag{2.1}$$

[1]This overly simple description is inaccurate in one main respect, which is that the hemispheric polewards circulation actually consists of three cells, not one: a tropical cell, a mid-latitude cell and a polar cell. The prevailing winds are westerly (from the west) only in the mid-latitude cells; tropical winds (the *trade* winds), for example, are easterlies (from the east).

A. Fowler, *Mathematical Geoscience*, Interdisciplinary Applied Mathematics 36,
DOI 10.1007/978-0-85729-721-1_2,

where σ is the Stefan–Boltzmann constant, given by $\sigma = 5.67 \times 10^{-8}\ \mathrm{W\,m^{-2}\,K^{-4}}$. If we assume that the Earth acts as a black body of radius R with *effective* (radiative) temperature T_e, and that it is in radiative *equilibrium*, then

$$4\pi R^2 \sigma T_e^4 = \pi R^2 (1-a) Q,$$

whence

$$T_e = \left[\frac{(1-a)Q}{4\sigma}\right]^{1/4}. \tag{2.2}$$

Computing this value for the Earth using the parameters above yields $T_e \approx 255$ K. A bit chilly, but not in fact all that bad!

Actually, if the average effective temperature is *measured* (T_m) via the black body law from direct measurements of emitted radiation, one finds $T_m \approx 250$ K, which compares well with T_e. On the other hand, the Earth's (average) surface temperature is $T_s \approx 288$ K. The fact that $T_s > T_e$ is due to the *greenhouse* effect, to which we will return later. First we must deal in some more detail with the basic mechanisms of radiative heat transfer.

2.2 Radiative Heat Transfer

We are familiar with the idea of conductive heat flux, a vector with magnitude and direction, which depends on position $\mathbf{r}$. Radiant energy transfer is a more subtle concept. A point in a medium will emit radiation of different frequencies ν (or different wavelengths λ: they are conventionally related by $\lambda = c/\nu$, where c is the speed of light), and the intensity of emitted radiation will depend not only on position $\mathbf{r}$, but also on *direction*, denoted by $\mathbf{s}$, where $\mathbf{s}$ is a *unit* vector. Also, like heat flux, emitted radiation is an area-specific quantity (i.e., it denotes energy emitted per unit area of emitting surface), and because it depends on orientation, this causes also a dependence on angle between emitting surface and direction: the intensity you receive from a torch depends on whether it is shone at you or not.

So, the *radiation intensity* $I_\nu(\mathbf{r}, \mathbf{s})$ is defined via the relation

$$dE_\nu = I_\nu \cos\theta \, d\nu \, dS \, d\omega \, dt, \tag{2.3}$$

where dE_ν is the energy transmitted in time dt through an area dS in the frequency range $(\nu, \nu + d\nu)$ over a *pencil* of rays of *solid angle* $d\omega$ in the direction $\mathbf{s}$; see Fig. 2.1. θ is the angle between $\mathbf{s}$ and $d\mathbf{S}$.

The solid angle (element) $d\omega$ is the three-dimensional generalisation of the ordinary concept of angle, and is defined in an analogous way. The solid angle $d\omega$ subtended at a point O by an element of surface area $d\mathbf{S}$ located at $\mathbf{r}$ is simply

$$d\omega = \frac{\mathbf{r} \,.\, d\mathbf{S}}{r^3}. \tag{2.4}$$

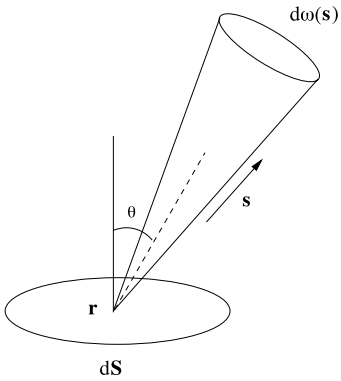

Fig. 2.1 A pencil of rays emitted from a point **r** in the direction of **s**

The solid angle subtended at O by a surface Σ is just $\omega = \int_\Sigma \frac{\mathbf{r}.d\mathbf{S}}{r^3}$, and for example $\int_\bigcirc d\omega = 4\pi$, representing the solid angle over all directions from a point, and $\int_\frown d\omega = 2\pi$, representing the solid angle subtended over all upward directions.

Three processes control how the intensity of radiation varies in a medium.

- *Absorption* occurs when a ray is absorbed by a molecule, e.g. of H_2O or CO_2 in the atmosphere, or by water droplets or particles. The rate of absorption is proportional to the density of the medium ρ and the radiation intensity I_ν, and is thus given by $\rho\kappa_\nu I_\nu$, where κ_ν is the *absorption coefficient*.
- *Emission* occurs (in all directions) when molecules or particles emit radiation; this occurs at a rate proportional to the density ρ, and is thus ρj_ν, where j_ν is the *emission coefficient*.
- *Scattering* can be thought of as a combination of absorption and emission, or alternatively as a local reflection. An incident ray on a molecule or particle—a *scatterer*—is re-directed (not necessarily uniformly) by its interaction with the scatterer. The process is equivalent to instantaneous absorption and re-emission. Reflection at a surface is simply the integrated response of a distribution of scatterers. Scattering leads to an effective scattering emission coefficient $j_\nu^{(s)}$, and is discussed further below in Sect. 2.2.6.

2.2.1 Local Thermodynamic Equilibrium

In order to prescribe j_ν, we will make the assumption of local thermodynamic equilibrium. More or less, this means that the medium is sufficiently dense that a local (absolute) temperature T can be defined, and *Kirchhoff's law* then defines j_ν as

$$j_\nu = \kappa_\nu B_\nu(T), \tag{2.5}$$

where $B_\nu(T)$ is the Planck function given by

$$B_\nu(T) = \frac{2h\nu^3}{c^2[e^{h\nu/kT} - 1]}, \tag{2.6}$$

where $h = 6.6 \times 10^{-34}$ J s is Planck's constant, $k = 1.38 \times 10^{-23}$ J K^{-1} is Boltzmann's constant, and $j_\nu \, d\nu$ represents the emitted energy per unit mass per unit time per unit solid angle in the frequency range $(\nu, \nu + d\nu)$. The formula (2.6) can be used to derive the Stefan–Boltzmann law (2.1) (see Question 2.2).

2.2.2 Equation of Radiative Heat Transfer

Considering Fig. 2.1, the rate of change of the radiation intensity I_ν in the direction $\mathbf{s}$ is given by

$$\frac{\partial I_\nu}{\partial s} = -\rho\kappa_\nu I_\nu + \rho\kappa_\nu B_\nu, \tag{2.7}$$

and this is the equation of radiative heat transfer. Note that the meaning of $\partial I_\nu/\partial s$ in (2.7) is that it is equal to $\mathbf{s}.\nabla I_\nu$, where ∇ is the gradient with respect to $\mathbf{r}$. (2.7) is easily derived from first principles, given the definition of absorption and emission coefficients.

2.2.3 Radiation Budget of the Earth

We will use (2.7) to derive a model for the vertical variation of the intensity of radiation in the Earth's atmosphere. We need to do this in order to explain the discrepancy between the effective black body temperature of the Earth (250 K) and the observed surface temperature (290 K). The discrepancy is due to the greenhouse effect of the atmosphere, which acts both as an absorber and emitter of radiation. Importantly, the absorptive capacity of the atmosphere as a function of wavelength λ is very variable. Figure 2.2 shows the variation of κ_ν (or, we might write κ_λ) as a function of λ, or more specifically, $\log_{10}\lambda$. Above it we have also the black body radiation curves for two temperatures corresponding to those of the effective Earth emission temperature, and to that at the surface of the Sun. (To obtain these, we write the Planck function as a density B_λ in wavelength λ, using the fact that $\nu = \frac{c}{\lambda}$, where c is the speed of light, thus $d\nu = -\frac{c\,d\lambda}{\lambda^2}$, and therefore we define

$$B_\lambda = \frac{cB_\nu}{\lambda^2} = \frac{2hc^2}{\lambda^5[e^{hc/k\lambda T} - 1]}.) \tag{2.8}$$

From the graphs in Fig. 2.2, we see that solar radiation is concentrated at short wavelengths, including the band of visible light ($\lambda = 0.4$–0.7 μm), whereas the emitted

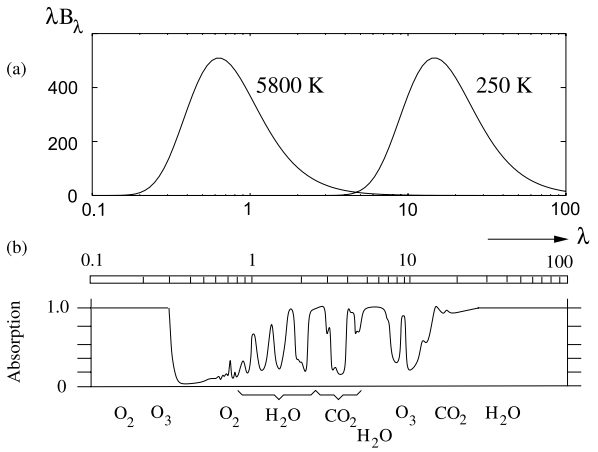

Fig. 2.2 Absorption spectrum of the Earth's atmosphere. The upper graphs indicate the different wavelength dependence of the radiation emitted by the Earth and the Sun. λ is measured in μm, and the solar output (from (2.8)) is scaled by 3.45×10^{-6} so that it overlays the Earth's output, if additionally λ in (2.8) is scaled by 0.043. In this case the areas under the two curves (note that $\int B_\lambda \, d\lambda = \ln 10 \int \lambda B_\lambda \, d \log_{10} \lambda$) are equal, as they should be in radiative balance. The factor 3.45×10^{-6} represents the product of $\frac{1}{4}(1 - a)$ (cf. (2.2)) with the square of the ratio of the Sun's radius to the distance from the Earth to the Sun. The radius of the Sun is 6.96×10^8 m and the distance from the Earth to the Sun is 1.5×10^{11} m, so that the value of the square ratio is about 21.53×10^{-6}. Multiplying this by the discount factor $\frac{1}{4}(1 - a)$ gives 3.45×10^{-6} if the albedo $a = 0.36$. The curves can be made to overlap for the measured albedo of $a = 0.3$ by, for example, taking Earth and Sun radiative temperatures to be 255 K and 5780 K, but this is largely a cosmetic exercise. The lower curve represents the absorption by atmospheric gases over a clear vertical column of atmosphere (i.e., it does not represent the absorption coefficient); we see that there is a long-wave window for wavelengths between about 8 and 15 μm. This figure is redrawn from Fig. 2.1 of Houghton (2002), by permission of Cambridge University Press

radiation is all infra-red (IR). Furthermore, the absorption coefficient variation with λ is such that the atmosphere is essentially *transparent* ($\kappa \approx 0$) to solar radiation (in the absence of clouds), but (mostly) *opaque* to the emitted long-wave radiation, with the exception of an IR window between 8 and 14 μm. It is this concept of transparency to solar radiation in the presence of only a small emission window, which leads to the analogy of a greenhouse.[2] The outgoing radiation is trapped by the atmosphere, and it is this which causes the elevated surface temperature.

The actual radiation budget of the Earth's atmosphere is shown in Fig. 2.3, which indicates the complexity of the transfer processes acting between the Earth's surface, the atmosphere and cloud cover, and which also shows the rôle played by *sensible* heat loss (i.e., due to convective or conductive cooling) and *latent* heat loss (due to evaporation from the oceans, for instance).

[2]The analogy is probably rather loose, since it is more the absence of convective (rather than radiative) cooling of the greenhouse which causes its elevated temperature.

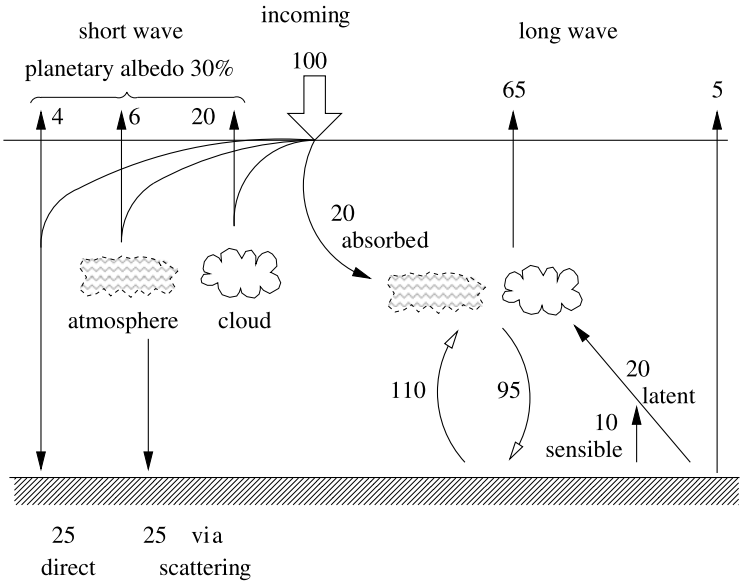

Fig. 2.3 Radiation budget of the Earth. Versions of this figure, differing slightly in the numerical values, can be found in many books. See, for example, Gill (1982), Fig. 1.6

As indicated in this figure, and as can be seen also from Fig. 2.2, one can essentially think of the short-wave budget and long-wave budget as separate systems. We shall be concerned here with the variation of IR radiation intensity, by solving (2.7). If κ_ν varies with ν, the problem requires computational solution. However, we can gain significant insight by introducing the idea of a *grey atmosphere*. This is one for which $\kappa_\nu = \kappa$ is independent of ν (and as mentioned, we will restrict this assumption to the long-wave budget).

We then define the radiation intensity I and emission density B as

$$I = \int_0^\infty I_\nu \, d\nu, \qquad B = \int_0^\infty B_\nu \, d\nu. \tag{2.9}$$

Note that we have

$$B = \frac{\sigma T^4}{\pi}, \tag{2.10}$$

where σ is the Stefan–Boltzmann constant; thus $B = E_b/\pi$. The factor of π arises because E_b represents the radiation per unit surface area emitted normally to the surface, while B represents emission per unit area per unit solid angle in any direction. It is important to understand the distinction between the two.

From (2.7), we have for a grey atmosphere

$$\frac{\partial I}{\partial s} = -\kappa\rho(I - B). \tag{2.11}$$

We now consider the important case of a one-dimensional atmosphere. Let z be the direction in the upward vertical, and let θ be the (polar) angle to the z-axis. We also define the optical depth

$$\tau = \int_z^\infty \kappa\rho \, dz, \tag{2.12}$$

and put $\mu = \cos\theta$. For a one-dimensional atmosphere, we have $I = I(\tau, \mu)$, where τ represents the vertical position, and μ represents the direction of the ray pencil in Fig. 2.1. Note also that $ds = dz/\mu$ (some care is needed here: z and s are independent, but this relation correctly interprets $\partial/\partial s \equiv \mathbf{s}.\nabla_{\mathbf{r}}$ for the one-dimensional case), so that (2.11) is

$$\mu \frac{\partial I}{\partial \tau} = I - B, \tag{2.13}$$

for a *one-dimensional, grey* atmosphere.

This seems simple enough, but note that B depends on T, which is as yet unconstrained. In order to constitute B, we define the *average intensity*

$$J = \frac{1}{4\pi} \int_\bigcirc I \, d\omega = \frac{1}{2} \int_{-1}^{1} I(\tau, \mu) \, d\mu, \tag{2.14}$$

and we make the assumption of *local radiative equilibrium*[3] that $J = B$, i.e., that the total absorbed radiation at a point is equal to that determined by black body emission (note that this does not necessarily imply $I = B$ for all θ, however). The radiative intensity equation for a one-dimensional, grey atmosphere is thus

$$\mu \frac{\partial I}{\partial \tau} = I - \frac{1}{2} \int_{-1}^{1} I(\tau, \mu) \, d\mu, \tag{2.15}$$

and is in fact an integro-differential equation.

We require two further pieces of information to determine I completely. In view of our previous discussion, we take I as referring to long-wave radiation, and therefore it is appropriate to specify

$$I = 0 \quad \text{for } \mu < 0 \text{ at } \tau = 0, \tag{2.16}$$

i.e., no incoming long-wave radiation at the top of the atmosphere. Furthermore, we can see from Eq. (2.15) that the net upward flux

$$\int_\bigcirc I \cos\theta \, d\omega = 2\pi \int_{-1}^{1} \mu I \, d\mu = \Phi \tag{2.17}$$

is conserved (i.e., is independent of depth). (The factor 2π is due to integration with respect to the azimuthal angle ϕ.) Since this is $2\pi[\int_0^1 \mu I \, d\mu - \int_{-1}^0 (-\mu I) \, d\mu] =$

[3] This now specifically assumes that no other energy transport processes occur.

outgoing IR radiation minus incoming IR radiation, it is in fact equal to the net emission of IR radiation. By the assumption of global radiative balance, Φ is equal to the net received short-wave radiation, thus

$$\Phi = \frac{(1-a)Q}{4} = \sigma T_e^4, \tag{2.18}$$

where the factor 4 allows for the variation of received solar radiation per unit area with latitude. (Strictly, the assumption of a one-dimensional atmosphere assumes horizontal variations due to latitude are rapidly removed, e.g. by mixing, but in fact the horizontal variation is small anyway, because the atmosphere is geometrically *thin*.) In fact, even if there is global imbalance, as in climatic energy-balance models (see Sect. 2.4), we still have $\Phi = \sigma T_e^4$.

2.2.4 The Schuster–Schwarzschild Approximation

The solution of (2.15) with (2.16) and (2.17) is possible but technically difficult, and is described in Appendix A. A simple approximate result can be obtained by defining the outward and inward flux integrals

$$\begin{aligned} I_+ &= \int_0^1 I \, d\mu, \\ I_- &= \int_{-1}^0 I \, d\mu, \end{aligned} \tag{2.19}$$

and then approximating $\int_0^1 \mu I \, d\mu \approx \frac{1}{2} I_+$, $\int_{-1}^0 \mu I \, d\mu = -\frac{1}{2} I_-$, based on the idea that $\int_0^1 \mu \, d\mu = \frac{1}{2}$. This causes (2.15) to be replaced by

$$\begin{aligned} I'_+ &= I_+ - I_-, \\ I'_- &= I_+ - I_- \end{aligned} \tag{2.20}$$

so that $I_+ - I_- = \Phi/\pi$ is the conservation law (2.17), and thus (with $I_- = 0$ at $\tau = 0$)

$$\begin{aligned} I_- &= \Phi\tau/\pi, \\ I_+ &= \frac{\Phi}{\pi}(1+\tau). \end{aligned} \tag{2.21}$$

It follows that the average intensity

$$J = \frac{1}{2}(I_+ + I_-) = \frac{\Phi}{2\pi}(1+2\tau) = B, \tag{2.22}$$

and using (2.10) and (2.18), we thus find the atmospheric temperature T in terms of the emission temperature T_e:

$$T = T_e\left[\frac{(1+2\tau)}{2}\right]^{1/4}. \tag{2.23}$$

The surface temperature is determined by the black body emission temperature corresponding to I_+ at the surface, where $\tau = \tau_s$, that is, $I_+ = B = \sigma T_s^4/\pi$, so that the ground surface temperature is

$$T_s = T_e(1+\tau_s)^{1/4}, \tag{2.24}$$

whereas the surface air temperature T_{as} is, from (2.23),

$$T_{as} = T_e\left(\frac{1}{2}+\tau_s\right)^{1/4}. \tag{2.25}$$

Note that there is a discontinuity in temperature at the surface, specifically

$$T_s^4 - T_{as}^4 = 0.5T_e^4; \tag{2.26}$$

molecular heat transport (conduction) will in fact remove such a discontinuity. If we use $T_s = 290$ K and $T_e = 255$ K, then (2.24) implies that the optical depth of the Earth's atmosphere is $\tau_s = 0.67$.

2.2.5 *Radiative Heat Flux*

Although radiative heat transfer is the most important process in the atmosphere, other mechanisms of heat transport are essential to the thermal structure which is actually observed, notably conduction and convection. In order to incorporate radiative heat transfer into a more general heat transfer equation, we need to define the *radiative heat flux*. This is a vector, analogous to the conductive heat flux vector, and is defined (for a grey medium) by

$$\mathbf{q}_R = \int_{\bigcirc} I(\mathbf{r},\mathbf{s})\,\mathbf{s}\,d\omega(\mathbf{s}). \tag{2.27}$$

Note that $\mathbf{q}_R.\mathbf{n} = \int_{\bigcirc} I\cos\theta\,d\omega$ (see Fig. 2.1) is the energy flux density through a surface element dS with normal $\mathbf{n}$. Determination of $\mathbf{q}_R$ requires the solution of the radiative heat transfer equation for I, but a simplification occurs in the optically dense limit, when $\tau \gg 1$ (i.e., $\kappa\rho$ is small). We write

$$I = B - \frac{1}{\rho\kappa}\mathbf{s}.\nabla I, \tag{2.28}$$

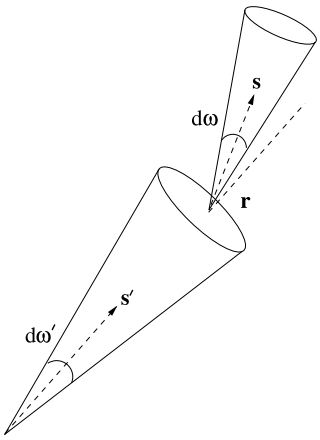

Fig. 2.4 Scattering from direction $\mathbf{s}'$ to $\mathbf{s}$

and solve for I using a perturbation expansion in powers of $1/\rho\kappa$. One thus obtains

$$I = B - \frac{1}{\rho\kappa}\mathbf{s}.\nabla B + \cdots, \tag{2.29}$$

and substitution into (2.27) leads to the expression

$$\mathbf{q}_R \approx -\frac{4\pi}{3\kappa\rho}\nabla B = -\frac{4\sigma}{3\kappa\rho}\nabla T^4, \tag{2.30}$$

so that for an optically dense atmosphere, the radiative heat flux is akin to a conductive heat flux, with a nonlinear temperature-dependent (radiative) conductivity. Because of its simplicity, we will often use this expression for the radiative flux despite its apparent inappropriateness for the Earth.

2.2.6 Scattering

In a scattering atmosphere, a beam of radiation is scattered as it is transmitted, as indicated in Fig. 2.4. At any position $\mathbf{r}$, an incident beam of frequency ν in the direction $\mathbf{s}'$ will be deflected to a new direction $\mathbf{s}$ with a probability distribution which we define to be $p_\nu(\mathbf{s}, \mathbf{s}')/4\pi$; thus the integral of p_ν over all directions is one, i.e.,

$$\int_{\bigcirc} p_\nu(\mathbf{s}, \mathbf{s}')\,\frac{d\omega(\mathbf{s}')}{4\pi} = 1. \tag{2.31}$$

If all the incident radiation is scattered, then we have perfect scattering: no radiation is lost. More generally, we may suppose that a fraction a_ν is scattered (and the rest is absorbed), and a_ν is called the albedo for single scattering. Thus we define $\frac{a_\nu p_\nu\, d\omega}{4\pi}$ to be the probability that incident radiation from the direction $\mathbf{s}'$ will be

scattered in the direction $\mathbf{s}$ over a solid angle increment $d\omega$. In general, p_ν depends on frequency, and we also suppose it depends only on the angle between $\mathbf{s}'$ and $\mathbf{s}$, thus $p_\nu = p_\nu(\mathbf{s}.\mathbf{s}')$.

Integrating this probability over all directions $\mathbf{s}'$, we obtain the emission coefficient for scattering as

$$j_\nu^{(s)} = a_\nu \kappa_\nu \int_{\bigcirc} p_\nu(\mathbf{s}, \mathbf{s}') I_\nu(\mathbf{r}, \mathbf{s}') \frac{d\omega(\mathbf{s}')}{4\pi}, \tag{2.32}$$

where κ_ν is the emission coefficient. The equation of radiative transfer is modified from (2.7) to

$$\frac{\partial I_\nu}{\partial s} = -\rho\kappa_\nu \left[I_\nu - (1 - a_\nu) B_\nu - a_\nu \int_{\bigcirc} p_\nu(\mathbf{s}, \mathbf{s}') I_\nu(\mathbf{r}, \mathbf{s}') \frac{d\omega(\mathbf{s}')}{4\pi} \right]. \tag{2.33}$$

Scattering in the atmosphere is most closely associated with Rayleigh's explanation for the blue colour of the sky. For the visible spectrum we can ignore shortwave emission, $B_\nu = 0$. Rayleigh derived an expression for the scattering distribution of sunlight by air molecules. Importantly, the intensity of scattered radiation is proportional to ν^4 (or $1/\lambda^4$), and thus is much larger for high frequency, or shortwavelength, radiation. In terms of the visible spectrum, this is the blue end. The wavelength of blue light is about 0.425 μm, while that of red light is 0.65 μm, so that blue light is scattered about five times more than red light. Hence the blue sky.

Rayleigh scattering applies to scattering by entities which are much smaller than the radiation wavelength, and in particular, molecules. Scattering by objects much larger than the wavelength (dust particles, water droplets, etc.) is called Mie scattering and is determined by WKB theory applied to the electromagnetic wave equation.

2.2.7 Troposphere and Stratosphere

Thus far, we have not considered the vertical structure of the atmosphere. The principal feature of the atmosphere is that it is stratified: the density decreases, more or less exponentially, with height. This is why it becomes difficult to breathe at high altitude. The reason for this decrease is simply that the atmospheric pressure at a point depends on the weight of the overlying air, which obviously decreases with height. Since density is proportional to pressure, it also decreases with height.

To quantify this, we use the fact that for a *shallow* atmosphere (whose depth d is much less than a relevant horizontal length scale l), the pressure p is nearly hydrostatic, that is,

$$\frac{dp}{dz} = -\rho g, \tag{2.34}$$

where z is height, ρ is air density, and g is gravitational acceleration (approximately constant). If we assume (reasonably) that air behaves as a perfect gas, then

$$\rho = \frac{M_a p}{RT}, \tag{2.35}$$

where M_a is the *molecular weight*[4] of air, R is the perfect gas constant, and T is absolute temperature. For a perfect gas, the thermal expansion coefficient $-\frac{1}{\rho}\frac{\partial \rho}{\partial T}$ is simply $1/T$.

In terms of the temperature, the pressure and density are then found to be

$$p = p_0 \exp\left[-\int_0^z \frac{dz}{H}\right], \qquad \rho = \rho_0 \exp\left[-\int_0^z \frac{dz}{H}\right], \tag{2.36}$$

where the *scale height* is

$$H = \frac{RT}{M_a g}, \tag{2.37}$$

having a value in the range 6–8 km. The temperature varies by less than a factor of two over most of the atmosphere, and an exponential relation between pressure or density and height is a good approximation.

We mentioned earlier, in deriving (2.15), that we assumed local radiative equilibrium, that is to say, radiative transport dominates the other transport mechanisms of convection and heat conduction. As we discuss further below, this is a reasonable assumption if the atmospheric density is small. As a consequence of the decrease in density with height, the atmosphere can therefore be divided into two layers. The lower layer is the *troposphere*, of depth about 10 km, and is where convective heat transport is dominant, and the temperature is *adiabatic*, and decreases with height: this is described in Sect. 2.3 below. The troposphere is separated from the *stratosphere* above it by the *tropopause*; atmospheric motion is less relevant in the stratosphere, and the temperature is essentially governed by radiative equilibrium. In fact the adiabatic decrease in temperature in the troposphere stops around the tropopause, and the temperature increases again in the stratosphere to about 270 K at 50 km height (the *stratopause*), before decreasing again (in the *mesosphere*) and then finally rising at large distances (in the *thermosphere*, >80 km).

The temperature structure of the atmosphere can thus be represented as in Fig. 2.5: the convection in the troposphere mixes the otherwise radiative temperature field to produce the adiabatic gradient which is observed.

[4]The molecular weight is effectively the weight of a molecule of a substance. Equivalently, it is determined by the weight of a fixed number of molecules, known as a *mole*, and equal to *Avogadro's number* 6×10^{23} molecules. For air, a mixture predominantly of nitrogen (78%), oxygen (21%) and argon (0.9%), the molecular weight is given by the equivalent quantity for the mixture. It has the value $M_a = 28.8 \times 10^{-3}$ kg mole^{-1}. Useful references for such quantities and their units are Kaye and Laby (1960) and Massey (1986).

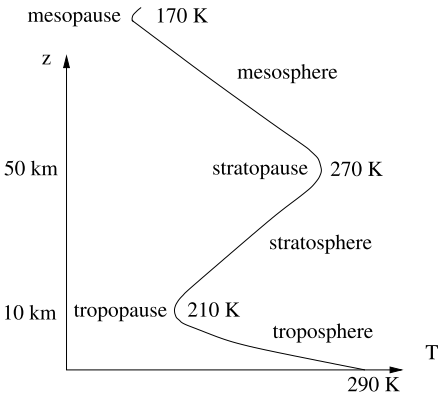

Fig. 2.5 Atmospheric temperature profile. Below the tropopause, convection stirs the temperature field into an adiabatic gradient. Above it, radiative balance is dominant

2.2.8 The Ozone Layer

The elevated vertical temperature profile in the stratosphere is basically due to a radiative balance between ultraviolet absorption by ozone and long wave emission by carbon dioxide. As is indicated in Fig. 2.2 (and as is well known), ozone (O_3) in the stratosphere is responsible for removing ultraviolet radiation, which would otherwise be lethal to life on Earth. Ozone is produced in the stratosphere through the photodissociation of oxygen. The basic sequence of reactions describing this process is due to Sydney Chapman:

$$\begin{aligned} O_2 + h\nu &\xrightarrow{j_2} 2O, \\ O + O_2 + M &\xrightarrow{k_2} O_3 + M, \\ O_3 + h\nu &\xrightarrow{j_3} O + O_2, \\ O + O_3 &\xrightarrow{k_3} 2O_2. \end{aligned} \tag{2.38}$$

The first of these reactions represents the breakdown of oxygen by absorption of ultraviolet radiation of wavelength less than 0.24 μm ($h\nu$ is Planck's quantum of energy). The next two reactions are fast. The arbitrary air molecule M catalyses the first of these. The final reaction represents the removal of ozone. Overall, the reaction can be written as

$$3O_2 \underset{r_-}{\overset{r_+}{\rightleftharpoons}} 2O_3, \tag{2.39}$$

with the first two reactions of (2.38) providing the forward reaction, and the last two the backward reaction. If we assume (as is the case) that j_3 and k_2 are sufficiently large that

$$\varepsilon = \frac{j_3}{k_2[O_2][M]} \ll 1, \qquad \delta = \left[\frac{j_2 k_3}{j_3 k_2[M]}\right]^{1/2} \ll 1, \tag{2.40}$$

then one can show (see Question 2.8) that the forward and backward rates for (2.39) are

$$r_+ = \frac{2}{3} j_2, \qquad r_- = \frac{j_3 k_3}{k_2[\mathrm{O}_2][\mathrm{M}]}, \tag{2.41}$$

and the (stable) equilibrium ozone concentration is given by

$$[\mathrm{O}_3] = \left[\frac{j_2 k_2 [\mathrm{M}]}{j_3 k_3} \right]^{1/2} [\mathrm{O}_2]. \tag{2.42}$$

Ozone occurs principally in the *ozone layer*, at heights between 15 and 50 km (i.e., in the stratosphere), where it attains concentrations of about 10 ppmv (parts per million by volume). It is formed here because the reactions in (2.38) require UV radiation to be absorbed, which in itself requires the presence of oxygen. So at the top of the stratosphere, where the pressure and thus also density are both small, absorption is small and little ozone is formed. Deeper in the stratosphere, density increases, which allows increased production of ozone, but also less UV radiation can penetrate to deeper levels, and so the source for the ozone forming reaction disappears at the base of the stratosphere. The ozone which is produced itself enhances the absorption of UV radiation, of course.

A simple model for the formation of this structure, which is called a *Chapman layer*, assumes a constant volume concentration, or mixing ratio, for ozone. The radiative transfer equation for incoming shortwave radiation of intensity I can be written

$$\frac{\partial I}{\partial z} = \kappa \rho I; \tag{2.43}$$

there is no radiative source term, and the incoming beam is unidirectional, and here taken to be vertical (the Sun is overhead). We suppose a constant pressure scale height so that

$$\rho = \rho_0 \exp(-z/H). \tag{2.44}$$

With I negative, and $I \to -I_\infty$ as $z \to \infty$, the solution to this is

$$I = -I_\infty \exp\left[-\kappa \rho_0 H e^{-z/H}\right], \tag{2.45}$$

and the consequent heating rate $Q = -\frac{\partial I}{\partial z}$ is given by

$$Q = \frac{\tau_0 I_\infty}{H} \exp\left[-\frac{z}{H} - \tau_0 e^{-z/H} \right], \tag{2.46}$$

where

$$\tau_0 = \kappa \rho_0 H \tag{2.47}$$

is a measure of the opacity of the stratospheric ozone layer.

If τ_0 is sufficiently high, the heating rate exhibits an internal maximum, as seen in Fig. 2.6. This is the distinguishing feature of the Chapman layer. Since Q is also

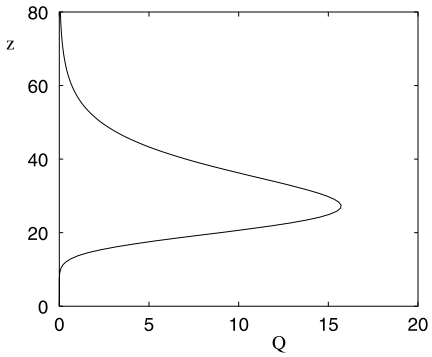

Fig. 2.6 Variation of heating rate Q given by (2.46) with $I_\infty = 342\ \mathrm{W\,m^{-2}}$, $H = 8$ km, and $\tau_0 = 30$, this somewhat arbitrary value being chosen to show a maximum heating rate at 30 km altitude. Units of z are km, and of $Q\ \mathrm{W\,m^{-3}}$. The choice of $I_\infty = 342\ \mathrm{W\,m^{-2}}$ refers to all incoming short wave radiation, whereas it is only a small fraction of this in the ultraviolet range which is absorbed in the stratosphere

volumetric absorption rate of radiation, it indicates maximal production of ozone in the stratosphere, as is found to be the case. This structure additionally explains why the temperature rises with height through the stratosphere, because of the increased heating rate.

In the stratosphere much of the short-wave absorption is due to ozone. There is very little water vapour. The resultant heating is almost exactly balanced by long-wave radiation, mostly from carbon dioxide, the remnant being from ozone again. While the resulting radiation balance controls the temperature, there is very little radiant energy lost. As can be seen from Fig. 2.2, the UV tail is taken off by ozone and oxygen, but the visible and infra-red spectrum passes through the stratosphere relatively unscathed.

In the troposphere, the water vapour concentration is much higher than that of ozone, which is virtually absent, and also of carbon dioxide. Although discussions of global warming are fixated by the greenhouse gases—carbon dioxide, methane, and so on, it needs to be borne in mind that water vapour is also a greenhouse gas, and is in fact the most important one. Adding to that the dominating influence of clouds and their somewhat mysterious influence on climate, one sees that an understanding of moisture is of principal concern in determining radiative processes in the troposphere.

2.3 Convection

We have seen that for a purely radiative atmosphere, a discontinuity in temperature occurs at the Earth's surface. Such a discontinuity does not occur in reality, because of molecular conduction. In fact, atmospheric motion causes heat transport in the troposphere to be more importantly due to convection rather than conduction—the

transport of heat is primarily due to the motion of the atmosphere itself. The temperature of the atmosphere is described by the heat equation

$$\rho c_p \frac{dT}{dt} - \beta T \frac{dp}{dt} = k\nabla^2 T - \nabla.\mathbf{q}_R, \tag{2.48}$$

where the terms represent, respectively, advection of heat, adiabatic (compression) heating, thermal conduction and radiative heat transfer. The time derivative d/dt is a *material derivative*, and represents the rate of change of a property following a fluid element. Thus, $dT/dt = 0$ means the temperature of a fluid element is conserved as it moves. It is related to the ordinary partial derivative by the relation

$$\frac{d}{dt} = \frac{\partial}{\partial t} + \mathbf{u}.\nabla, \tag{2.49}$$

where $\mathbf{u}$ is the fluid velocity, c_p is the specific heat, $\beta = -\rho^{-1}\partial\rho/\partial T$ is the thermal expansion coefficient, k is the thermal conductivity, and $\mathbf{q}_R$ was defined above in (2.27).

If we use the optically dense approximation (2.30), then

$$\mathbf{q}_R \approx -k_R \nabla T, \tag{2.50}$$

where

$$k_R = \frac{16\sigma T^3}{3\kappa\rho}. \tag{2.51}$$

We will use (2.50) as a pedagogic tool rather than as an accurate model. To estimate k_R, we use values $\kappa\rho d = 0.7$, $d = 10$ km; then we find $k_R \sim 10^5$ W m^{-1} K^{-1}. This compares to a molecular thermal conductivity of order 10^{-2} W m^{-1} K^{-1}, which is therefore negligible. In fact, atmospheric flows are turbulent, and a better measure of the effective heat conduction is the eddy thermal conductivity, of order $\rho c_p U d$ times a small dimensionless drag coefficient, where d is depth scale and U is wind speed scale. This is discussed further in Chap. 3; we find that eddy conductivity is found to be comparable to the nominal radiative value deduced above.

A measure of the importance of the advective terms is provided by the *Péclet number*, which represents the size of the ratio $(\rho c_p\, dT/dt)/\nabla.\mathbf{q}_R$, and is given by

$$Pe = \frac{\rho c_p U d^2}{k_R l}, \tag{2.52}$$

where U and d are velocity and depth scales as mentioned above, and l is a relevant horizontal length scale. Using values $\rho \sim 1$ kg m^{-3}, $c_p \sim 10^3$ J kg^{-1} K^{-1}, $U \sim 20$ m s^{-1}, $d \sim 10$ km, $l \sim 10^3$ km (representing the length scale of planetary waves in the atmosphere), we find $Pe \sim 20$, so that in fact atmospheric motion plays a significant rôle in the redistribution of heat. Since Pe is large, we can obtain an approximation to the vertical thermal structure of the atmosphere by neglecting the

radiative and conductive transport terms altogether. This leads to the *adiabatic lapse rate*, which is determined by putting the left hand side of (2.48) to zero, and thus

$$\frac{dT}{dp} = \frac{\beta T}{\rho c_p}. \tag{2.53}$$

To obtain the variation of T with height z, we use the fact that the pressure is hydrostatic, given by (2.34), and assume a perfect gas law (2.35); then we find the (dry) adiabatic lapse rate

$$\frac{dT}{dz} = -\Gamma_d = -\frac{g}{c_p}, \tag{2.54}$$

having a value of about 10 $\mathrm{K\,km^{-1}}$. In practice, the observed temperature gradient is nearer 6 $\mathrm{K\,km^{-1}}$, a value which is due to the presence of water vapour in the atmosphere, the effect of which is considered below.

One of the basic reasons for the presence of convection in the troposphere is the presence of an unstable thermal gradient. The higher temperature at the ground causes the air there to be lighter; convection occurs as the warm air starts to rise, and it is the resultant overturning which causes the mixing which creates the adiabatic gradient. On a larger scale, and as we discuss further in Chap. 3, the unstable thermal gradient which drives large scale atmospheric motion is due to the energy imbalance between the equator and the poles.

Perturbations to the adiabatic gradient occur; for example, temperature inversions can occur under clear skies at night when IR radiation from the Earth is larger. The resultant temperature structure is convectively stable (the inversion is cold and therefore heavy), and its removal by solar irradiation can be hampered by the presence of smog caused by airborne dust particles. Moreover, the cool inversion causes fog (condensed water vapour), and the condensation is also facilitated by airborne pollutant particles, which act as nucleation sites. Hence the infamous smogs in London in the 1950s, and the consequent widespread ban of open coal fires in cities.

While temperature inversions are convectively stable and thus persistent, superadiabatic temperatures are convectively unstable, and cannot be maintained.

2.3.1 The Wet Adiabat

For a parcel of air of density ρ_a containing water vapour of density ρ_v, the *mixing ratio* is defined as

$$m = \frac{\rho_v}{\rho_a}. \tag{2.55}$$

A typical value in the troposphere is $m \approx 0.02$, so that we can practically take the density of moist air as constant. As m increases, the air can become *saturated* and thus the water vapour will condense. This happens when the *partial pressure* p_v

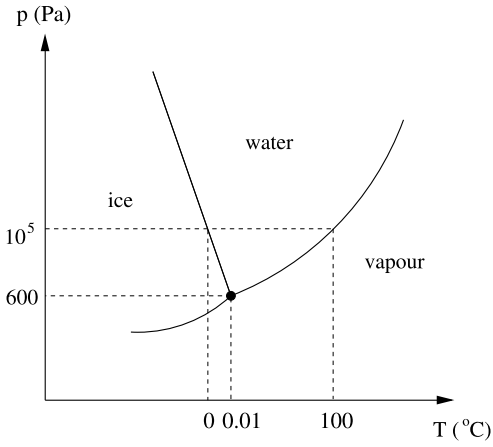

Fig. 2.7 Phase diagram for water substance (not to scale)

reaches the *saturation vapour pressure* p_{sv}, which depends on temperature via the Clausius–Clapeyron equation

$$\frac{dp_{sv}}{dT} = \frac{\rho_v L}{T}, \tag{2.56}$$

where L is the latent heat and T in (2.56) is the saturation value T_{sat}. Figure 2.7 shows the phase diagram for water, delineating the curves in (T, p) space at which freezing, condensation and sublimation occur. (2.56) describes the water/vapour curve in this figure. The ratio p_v/p_{sv} (normally measured as a percentage) is called the *relative humidity*. It is an anthropocentric measure of discomfort, since when the (relative) humidity is high, very little exertion will cause one to sweat.

Let us now suppose that the atmosphere is (just) saturated. The existence of clouds actually negates this proposition, but not too badly, in the sense that we suppose rainfall removes condensed water droplets. As a moist parcel of air moves about, the increment of heat content per unit volume due to changes in T, p and ρ_v is then $\rho_a c_p\, dT - dp + L\, d\rho_v$ (using $\beta T = 1$), and thus (2.48) is modified to

$$\rho_a c_p \frac{dT}{dt} - \frac{dp}{dt} + \rho_a L \frac{dm}{dt} = k\nabla^2 T - \boldsymbol{\nabla}.\mathbf{q}_R. \tag{2.57}$$

Using the definition of m in (2.55), and the perfect gas laws

$$p = \frac{\rho_a RT}{M_a}, \qquad p_{sv} = \frac{\rho_v RT}{M_v}, \tag{2.58}$$

where M_v is the molecular weight of water vapour, we find that the temperature gradient is given approximately (by ignoring the right hand side of (2.57)) by

$$\frac{dT}{dz} = -\Gamma_w = -\Gamma_d \left[\frac{1 + \frac{\rho_v L}{p}}{1 + \frac{\rho_v L}{p}\left(\frac{M_v}{M_a}\frac{L}{c_p T}\right)} \right], \tag{2.59}$$

which is the wet adiabat. Using values $\rho_v = 0.01\ \mathrm{kg\,m^{-3}}$, $M_v = 18 \times 10^{-3}\ \mathrm{kg\,mole^{-1}}$, $M_a = 28.8 \times 10^{-3}\ \mathrm{kg\,mole^{-1}}$, $L = 2.5 \times 10^6\ \mathrm{J\,kg^{-1}}$, $c_p = 10^3\ \mathrm{J\,kg^{-1}\,K^{-1}}$, $p \approx 10^5$ Pa, $T \approx 300$ K, we find a typical value $\Gamma_w \approx 5.4\ \mathrm{K\,km^{-1}}$, close to that which is observed in practice.

2.4 Energy Balance Models

Although convective transport is the dominant mechanism of energy transfer *within* the atmosphere, the rôle of radiative transport is fundamental to the determination of the average temperature. Moreover, this is equally true if we do *not* assume radiation balance, and this allows us to study long term variations in climate which are of relevance to the evolution of paleoclimatic temperatures, quaternary ice age climates, and more recently, the effect of CO_2 levels on global temperature. All of these phenomena can be roughly understood on the basis of *energy-balance models*.

Since most of the mass of the atmosphere is contained in the troposphere, we define the mean temperature $\bar{T}$ of the atmosphere to be the vertically averaged temperature of the troposphere. Suppose the temperature is adiabatic, with constant lapse rate Γ, and of depth d. The surface temperature T is thus

$$T = \bar{T} + \frac{1}{2}\Gamma d. \tag{2.60}$$

In a purely radiative atmosphere, we found earlier that the greenhouse effect causes the surface temperature to be warmer than the planetary long-wave emission temperature (cf. (2.24)). Let us define a greenhouse factor

$$\gamma = \left(\frac{T_e}{T}\right)^4, \tag{2.61}$$

where for (2.24), this would be

$$\gamma = \frac{1}{1+\tau_s}; \tag{2.62}$$

this enables us to write the emitted long-wave radiation in terms of the mean surface temperature, and a quantity γ which depends on atmospheric radiative properties.

We can still define a greenhouse factor by (2.61) for a radiative-convective atmosphere, but consultation of Fig. 2.3 shows that its theoretical determination in terms of atmospheric properties is likely to be non-trivial. Nevertheless, we shall suppose γ can be defined; for the Earth $\gamma \approx 0.61$ at present (based on $T_e = 255$ K, $T = 288$ K).

The incoming solar radiation per unit area is $(1-a)Q$ (a is the albedo, the fraction of short-wave radiation which is reflected back to space), while the emitted IR radiation per unit area is σT_e^4 (units are $\mathrm{W\,m^{-2}}$). It follows that the net received radiation over the planetary surface is $\pi R^2(1-a)Q - 4\pi R^2 \sigma T_e^4$, with units of

W, and we can equate this to the rate of change of the atmospheric heat content,[5] $4\pi R^2 d\rho_a c_p \frac{d\bar{T}}{dt}$, where d is the depth of the troposphere; c_p is the specific heat, and R is the planetary radius. Since $\rho_a R^2 d$ has units kg, c_p has units $\mathrm{J\,kg^{-1}\,K^{-1}}$, and dT/dt has units $\mathrm{K\,s^{-1}}$, this also has units W, and thus (adopting (2.61))

$$\rho_a c_p d\frac{dT}{dt} = \frac{1}{4}(1-a)Q - \sigma\gamma T^4, \tag{2.63}$$

in view of (2.60), since we take $\frac{1}{2}\Gamma d$ to be constant.

For constant Q, (2.63) is a simple first order differential equation with stable positive steady state, the radiative equilibrium state

$$T = T_0 = \left[\frac{(1-a)Q}{4\sigma\gamma}\right]^{1/4}. \tag{2.64}$$

The response time for small deviations from T_0 is then determined by the linearised equation, where we put $T = T_0 + \theta$, whence

$$\frac{\rho_a c_p d T_0}{(1-a)Q}\dot{\theta} \approx -\theta, \tag{2.65}$$

and the response time is

$$t_R \sim \frac{\rho_a c_p T_0 d}{(1-a)Q}. \tag{2.66}$$

With a density $\rho_a = 1\ \mathrm{kg\,m^{-3}}$, $c_p = 10^3\ \mathrm{J\,kg^{-1}\,K^{-1}}$, $T_0 = 288$ K, $d = 10^4$ m, $a = 0.3$, $Q = 1370\ \mathrm{W\,m^{-2}}$, we have $t_R \sim 35$ days, so that climatic response is relatively rapid.

2.4.1 Zonally Averaged Energy-Balance Models

Energy balance models are obviously crude, but attractive nonetheless because they portray the essential truth about atmospheric energy balance. One of the more obvious features of the planetary climate is the temperature difference between equator and poles, due to the latitudinal variation of received solar variation. Indeed, it is this imbalance which drives the atmospheric weather systems, as we shall see in Chap. 3. A simple modification to the 'zero-dimensional' energy-balance model (2.63) is to allow a latitudinal variation in temperature. We denote latitude (angle north of the equator) by λ and we define

$$\xi = \sin\lambda, \tag{2.67}$$

[5] This is something of a simplification. Net addition of radiant energy to the atmosphere can cause changes in sensible heat (via temperature), latent heat (via moisture) or gravitational potential energy (via thermal expansion); we thus implicitly neglect the latter two; see also Eq. (3.25) in Sect. 3.2.3, and the next footnote.

thus $-1 < \xi < 1$, and $\xi = 0$ at the equator, $\xi = 1$ at the north pole. We suppose $T(\xi, t)$ is the *zonally averaged* (i.e., integrated over longitude) temperature, and we pose the zonally averaged energy-balance equation

$$C\frac{\partial T}{\partial t} = D\frac{\partial}{\partial \xi}\left[\left(1-\xi^2\right)\frac{\partial T}{\partial \xi}\right] + \frac{1}{4}Q(1-a)S(\xi) - I(T). \tag{2.68}$$

In this equation, C is a heat capacity coefficient. For a dry atmosphere,[6] (2.63) indicates $C = \rho_a c_p d$. D is an effective thermal conduction coefficient, scaled with d/R^2, and thus having units of $\mathrm{W\,m^{-2}\,K^{-1}}$; it represents the poleward transport of energy through the eddy diffusive effect of large weather systems in mid-latitudes, which will be discussed further in the following chapter. $I(T)$ represents the outgoing long-wave radiation, supposed to depend only on mean surface temperature. Finally, $S(x)$ represents the latitudinal variation of received solar radiation, normalised so that $\int_0^1 S(\xi)\,d\xi = 1$. If the albedo a is constant, then we regain (2.63) by integrating from $\xi = -1$ to $\xi = 1$, assuming T is regular at the poles. If $S \equiv 1$, then $T = T(t)$, and we also regain the earlier model.

In the formulation of (2.68), we again interpret T as the mean surface temperature, in view of (2.60), and this is what is conventionally done, though without explicit mention. It is also conventional, in view of the limited range of T, to take a linear dependence of I on T, thus

$$I = A + BT, \tag{2.69}$$

with values of A and B from measurements. Typical such values[7] are $A = 200\ \mathrm{W\,m^{-2}}$ and $B = 2\ \mathrm{W\,m^{-2}\,K^{-1}}$.

The resulting linear equation for T can then be solved as a Fourier–Legendre expansion if the albedo is known. For example, let us suppose that a as well as S is an even function of ξ (thus exhibiting north-south symmetry). It is convenient to write Eq. (2.68) in terms of I, thus

$$C^*\frac{\partial I}{\partial t} = D^*\frac{\partial}{\partial \xi}\left[\left(1-\xi^2\right)\frac{\partial I}{\partial \xi}\right] + \frac{1}{4}Q(1-a)S(\xi) - I, \tag{2.70}$$

where $D^* = D/B$, $C^* = C/B$. We solve this in the steady state by writing

$$I = \sum_{n\ \text{even}} i_n P_n(\xi), \tag{2.71}$$

[6] For a moist, saturated atmosphere, we may take the moisture mixing ratio m to be a function of T, and in this case the latent heat $\rho_a L m$ (L being latent heat) simply modifies the heat capacity coefficient. Question 2.11 shows how to calculate $m(T)$. See also Sect. 3.2.7.

[7] The value of A assumes T is measured in degrees Celsius.

where P_n is the n-th Legendre polynomial (and is an even function of ξ for n even). If we expand

$$\frac{1}{4}Q(1-a)S(\xi) = \sum_{n \text{ even}} q_n P_n(\xi), \tag{2.72}$$

where

$$q_n = \frac{(2n+1)Q}{4}\int_0^1 (1-a)S(\xi)P_n(\xi)\,d\xi, \tag{2.73}$$

then the coefficients i_n are given by

$$i_n = \frac{q_n}{1+n(n+1)D^*}. \tag{2.74}$$

For example, if we take a to be constant and the realistic approximation $S = 1-\alpha P_2(\xi)$, $\alpha \approx 0.48$, then

$$I = \frac{1}{4}Q(1-a)\left[1 - \frac{\alpha P_2(\xi)}{1+6D^*}\right]. \tag{2.75}$$

A better approximation uses $a = a_0 + a_2 P_2(\xi)$, where $a = 0.68$ and $a_2 = -0.2$; this represents to some extent the higher albedo (due to ice cover) in the polar regions. The resultant two term approximation for the temperature, $T = (i_0 - A + i_2 P_2(\xi))/B$, then yields a good approximation to the observed mean surface temperature if we take $D = 0.65\ \mathrm{W\,m^{-2}\,K^{-1}}$.

2.4.2 Carbon Dioxide and Global Warming

If we are interested in the gradual evolution of climate over long time scales, then in practice we can neglect the time derivative term in (2.63), and suppose that T is in a quasi-equilibrium state. Figure 2.8 shows the rising concentration of CO_2 in the atmosphere over the last two hundred years. Essentially, the secular rise is due to the increased industrial output since the industrial revolution.

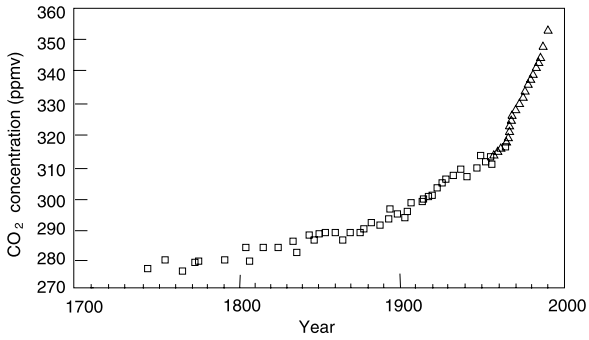

Fig. 2.8 Rise in atmospheric concentration of CO_2 since 1750. The *squares* indicate measurements from Antarctic ice cores, and the *triangles* represent direct measurements from Mauna Loa observatory in Hawaii

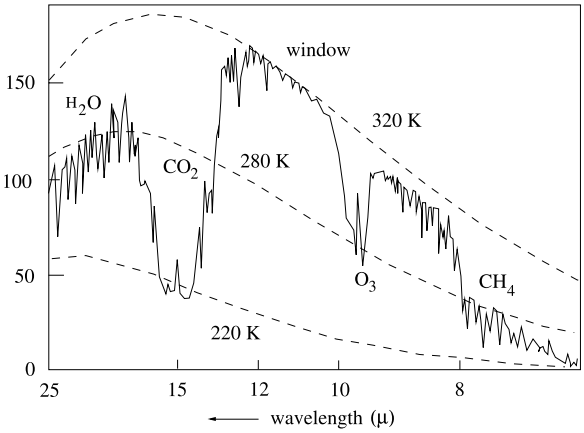

Fig. 2.9 Vertical thermal emission from the Earth measured over the Sahara. The *horizontal axis* is linear in wave number, hence the irregular intervals for the wavelength in microns. The units of radiation are $\mathrm{mW\,m^{-2}\,sr^{-1}\,(cm^{-1})^{-1}}$, the last two indicating inverse steradian (the unit of solid angle) and wave number. The *dashed lines* are the black body radiation curves at the indicated temperatures. Redrawn from Fig. 12.7 of Houghton (2002), by permission of Cambridge University Press

Although CO_2 is only present in small quantities, it is an important absorber for the long-wave emitted IR radiation. The effect of increasing its concentration is to increase the optical density, and thus to decrease γ. Let us suppose then that the change in CO_2 leads to a change in the greenhouse coefficient γ given by

$$\gamma = \gamma_0 - \tilde{\gamma}; \tag{2.76}$$

γ_0 is the pre-industrial reference state, and $\tilde{\gamma}$ represents the (positive) secular change due to CO_2. With $\tilde{\gamma} \ll 1$, we thus have the quasi-equilibrium given by (2.64), which leads to

$$T \approx T_0 + \frac{\tilde{\gamma} T_0}{4\gamma_0}. \tag{2.77}$$

Of course the difficulty lies in evaluating an effective dependence of $\tilde{\gamma}$ on CO_2 levels, and in reality, the problem is made more difficult by the non-greyness of the atmosphere. To understand this, let us consider the long-wave thermal emission as a function of wavelength. This is shown in Fig. 2.9, together with black body irradiance curves at various temperatures. The emission curve divides quite neatly into a number of distinct wavelength intervals, in each of which the emission quite closely follows the black body radiation corresponding to distinct temperatures. We see a window between 10 and 13 μ, where there is little absorption, and the effective emission temperature is that at ground level. At higher wavelength, (14–16 μ), there is a CO_2 absorption band, and the radiation appears to emanate from the lower stratosphere.

In order to understand how this can be, we revisit the concept of the Chapman layer discussed above in Sect. 2.2.8. We write the radiation intensity equation (2.7) for a one-dimensional atmosphere in the form

$$\mu \frac{\partial I_\nu}{\partial z} = -\kappa_\nu \rho_0 e^{-z/H}[I_\nu - B_\nu], \tag{2.78}$$

where H is the scale height, taken as constant. For local thermodynamic equilibrium, $B_\nu(T)$ is an increasing function of temperature given by (2.6). When $\mu = 1$, the solution for upwards travelling radiation is

$$I_\nu = I_\nu^0 \exp\left[-\tau_\nu\left(1 - e^{-\zeta}\right)\right] + \tau_\nu \exp\left[\tau_\nu e^{-\zeta}\right] \int_0^\zeta B_\nu(T) \exp\left[-\zeta - \tau_\nu e^{-\zeta}\right] d\zeta, \tag{2.79}$$

where

$$\zeta = z/H, \qquad \tau_\nu = \kappa_\nu \rho_0 H. \tag{2.80}$$

When τ_ν is small, as for the window between 10 and 13 μ, then

$$I_\nu \approx I_\nu^0. \tag{2.81}$$

When $\tau_\nu > 1$ the kernel of the integrand has an internal maximum at $\zeta = \ln \tau_\nu$, and by putting

$$\zeta = \ln \tau_\nu + Z, \tag{2.82}$$

we have for large τ_ν the approximation

$$I_\nu \approx \exp\left[e^{-Z}\right] \int_{-\ln \tau_\nu}^{Z} B_\nu(T) \exp\left[-Z' - e^{-Z'}\right] dZ'. \tag{2.83}$$

The kernel $\exp[-Z' - e^{-Z'}]$ of the integrand is a peaked function with a maximum at $Z' = 0$. It thus filters out the values of B in the vicinity of $\zeta = \ln \tau_\nu$. If we idealise the kernel as a delta function centred on $\zeta = \ln \tau_\nu$, then we have

$$I_\nu|_{Z\to\infty} \approx B_\nu(T)|_{\zeta = \ln \tau_\nu}, \tag{2.84}$$

and it is in this sense that the thermal emission picks out black body radiation at the level corresponding to the opacity at that frequency.

We denote the effective emission altitude for a particular frequency as z_ν, thus

$$z_\nu = H \ln[\kappa_\nu \rho_0 H]. \tag{2.85}$$

Inspection of Fig. 2.9 then suggests that the variation of z_ν with frequency (or wavelength) in the 15 μ CO_2 absorption band is as indicated in Fig. 2.10, this variation being due to the variation of absorption coefficient with ν.

We can now infer the effect of increasing CO_2 density. Increasing ρ_0 has the effect of shifting the emission altitude upwards. In the stratosphere, this increases the

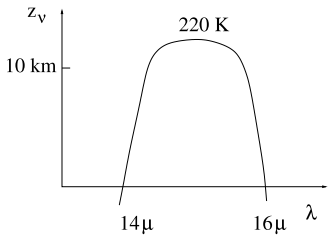

Fig. 2.10 Schematic variation of the effective emission height with wavelength in the CO_2 absorption band

temperature and therefore also the emission rate. Because of this, the stratosphere will cool under increased CO_2. On the other hand, the upwards shift of emission height at the fringes of the absorption band causes a cooling in the adiabatic troposphere and thus decreased emission. It is this shift of the emission height which is the cause of tropospheric heating under raised CO_2 levels.

Estimates of the consequential effect of increasing CO_2 levels is rendered uncertain because of various feedback effects which will occur in association. In particular, water vapour is also a major greenhouse gas (as can be seen from Fig. 2.9), and increased temperature causes increased evaporation and thus enhances the greenhouse effect. Perhaps more importantly, change of cloud cover can have a strong effect on temperature, because of its multiple influences: short-wave albedo, as well as long-wave absorption and emission (see Fig. 2.3). It is partly because of the uncertainty in parameterising cloud formation and structure that there is so much uncertainty associated with forecasts of global warming. Current estimates suggest that doubling CO_2 leads to a global increase of surface temperature in the region of 2–4 K. It has become popular to relate recent anomalous weather patterns (hurricane frequency, floods and heat waves, for example) to the effects of CO_2, but although this may indeed be the cause, nevertheless the natural variability of climate on short time scales does not allow us to make this deduction with any real justification. An alternative viewpoint is that since we know that CO_2 causes warming, it is a likely consequence that weather patterns will tend to become more variable, and it would then be of little surprise if this is actually happening. Indeed, the retreat of the glaciers since the nineteenth century is consistent with (but does not prove) the idea that global warming is not a recent phenomenon.

2.4.3 The Runaway Greenhouse Effect

If the blanketing effect of the greenhouse gases is the cause of the Earth's relatively temperate climate, what of Venus? Its surface temperature has been measured to be in the region of 700 K, despite (see Question 2.1) an effective emission temperature of 230 K. That the discrepancy is due to the greenhouse effect is not in itself surprising; the atmosphere is mostly CO_2 and deep clouds of sulphuric acid completely cover the planet. What is less obvious is why the Venusian atmosphere should have evolved in this way, since in other respects, Venus and Earth are quite similar planets.

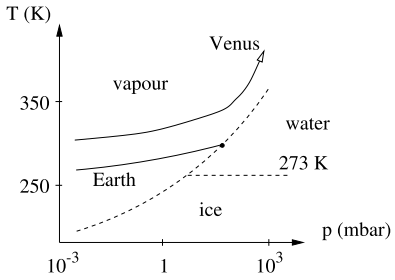

Fig. 2.11 A schematic representation of the evolution of temperatures on Venus and Earth. As the atmospheric water vapour increases on Earth, condensation occurs, leading to clouds, rainfall and ocean formation. On Venus this does not occur, and the water vapour is ultimately lost through dissociation, hydrogen escape and surface oxidation reactions

A possible explanation can be framed in terms of the simple energy-balance model proposed above, together with a consideration of the evolution of the amount of water vapour in the atmosphere. Initially, primitive terrestrial planets have no atmosphere (and no oceans or land ice). The internal heat generated by planetary accretion and by radioactive heat release is, however, substantial, and causes a huge amount of volcanism. In the eruption of magma, dissolved gases including H_2O and CO_2 are exsolved (for example, by pressure release, in much the same way bubbles form when a champagne bottle is opened). On the Earth, the increasing atmospheric density causes a slow rise in the temperature, while simultaneously the increasing partial pressure p_v of water vapour brings the atmosphere closer to saturation. On the Earth, it is supposed (see Fig. 2.11) that p_v reaches the saturation vapour pressure p_{sv} when $p_v > 600$ Pa (the triple point pressure). Clouds form of water droplets, and the ensuing rain forms the oceans and rivers. Most of the CO_2 is then removed from the atmosphere to form carbonate rocks.

On Venus, on the other hand, the slightly higher received solar radiation causes the (T, p_v) path which is traced to be higher. As p_v increases, so does T, and we suppose (see Fig. 2.11) that saturation never occurs. The water vapour continues to increase, leading to ever higher greenhouse temperatures.

A subsidiary question is then, what happens to the H_2O on Venus? The atmosphere is essentially devoid of H_2O. Here the idea is that UV radiation in the upper atmosphere dissociates the hydrogen from oxygen, the hydrogen then escapes to space, while the oxygen is used up in oxidising reactions with surface rocks.

The mechanism above is attractively simple, and can be understood using the concept of radiation balance in a grey atmosphere. The equilibrium temperature from (2.64) is

$$T = \left[\frac{(1-a)Q}{4\sigma\gamma}\right]^{1/4}, \tag{2.86}$$

and we can expect both the albedo a and greyness γ to depend on the density of water vapour ρ_v. For simplicity, take $a = 0$ and for γ we use a formula suggested

by (2.62) in the optically dense limit ($\tau_s \gg 1$):

$$\gamma = \frac{1}{\tau_s}. \tag{2.87}$$

Taking $\tau_s = \kappa \rho_v d$, we then have

$$T \approx \left[\frac{Q\kappa d}{4\sigma} \rho_v \right]^{1/4}, \tag{2.88}$$

and using the perfect gas law (2.58) in the form $p_v = \rho_v RT/M_v$ gives

$$T \approx \left[\frac{Q\kappa d M_v}{4\sigma R} p_v \right]^{1/5}, \tag{2.89}$$

and we write this in the form

$$T = \left[\frac{Q\kappa d M_v p_{sv}^0}{4\sigma R} \right]^{1/5} e^{\xi}, \tag{2.90}$$

where

$$\xi = \frac{1}{5} \ln\left(p_v / p_{sv}^0\right), \tag{2.91}$$

and p_{sv}^0 is a reference value of the saturation vapour pressure, which we will take to be the triple point pressure, 6 mbar. On the other hand, the saturation temperature is determined by solving the Clausius–Clapeyron equation (2.56). The exact solution of this is

$$p_{sv} = p_{sv}^0 \exp\left[a \left\{ 1 - \frac{T_{\text{sat}}^0}{T_{\text{sat}}} \right\} \right], \tag{2.92}$$

where T_{sat} is the saturation temperature, $a = M_v L / R T_{\text{sat}}^0$, and for $T_{\text{sat}} - T_{\text{sat}}^0 \ll T_{\text{sat}}^0$, this is

$$T_{\text{sat}} \approx T_{\text{sat}}^0 [1 + \nu \xi], \tag{2.93}$$

where

$$\nu = \frac{5}{a} = \frac{5RT_{\text{sat}}^0}{M_v L}, \tag{2.94}$$

with approximate value $\nu \approx 1/4$. T_{sat}^0 is the saturation temperature at the triple point, $T_{\text{sat}}^0 \approx 273$ K. If we write $T_{\text{sat}} = T_{\text{sat}}^0 \theta_{\text{sat}}$, $T = T_{\text{sat}}^0 \theta$, then the planetary and saturation temperature curves are given, respectively, by

$$\begin{aligned} \theta &= r e^{\xi}, \\ \theta_{\text{sat}} &= 1 + \nu \xi, \end{aligned} \tag{2.95}$$

where

$$r = \frac{1}{T_{\text{sat}}^0}\left[\frac{Q\kappa d M_v p_{sv}^0}{4\sigma R}\right]^{1/5}. \tag{2.96}$$

The definition of r here should not be taken too seriously, as we implicitly assumed that absorption was entirely due to water vapour. However, the intersection of the curves in (2.95) makes the point that the runaway effect can be expected if r is large enough, specifically if

$$r > r_c = \nu \exp\left(\frac{1-\nu}{\nu}\right) \approx 5 \tag{2.97}$$

for $\nu = 1/4$, and this corresponds to a sufficiently large value of Q. Hence, the distinction between Earth and Venus, for which the value of Q is twice that of Earth. The situation is illustrated in Fig. 2.11.

2.5 Ice Ages

Most people are probably aware that we live in glacial times. During the last two million years, a series of ice ages has occurred, during which large ice sheets have grown, principally on the northern hemisphere land masses. The Laurentide ice sheet grows to cover North America down to the latitude of New York, while the Fennoscandian ice sheet grows in Scandinavia, reaching into the lowlands of Germany, and possibly connecting across the north sea to a British ice sheet which covers much of Britain and Ireland down to Kerry in the west and Norfolk in the east. The global ice volume which grows in these ice ages is sufficient to lower sea level by some 120 metres, thus exposing vast areas of continental shelf.

These Pleistocene ice ages occur with some regularity, with a period of 100,000 years (although prior to the last 900,000 years, a periodicity of 40,000 years appears more appropriate). The great ice sheets grow slowly over some 90,000 years, and there is then a fairly sudden deglaciation. This is illustrated in Fig. 2.12, which shows a proxy measurement of temperature over the last 740,000 years, obtained from an Antarctic ice core. Five sharp rises in temperature can be seen separating the last four ice ages, which show a characteristic slow decline in temperature. As we shall see, the mechanism which causes this sequence of pseudo-periodic oscillations in the climate is not very well understood.

The present glacial climate may be a result of a gradual cooling initiated by the collision of India with Asia starting some 50 million years ago, and causing the rise of the Himalayas. Although these mountains affect weather systems directly, their effect on climate may be due to the increasing precipitation and thus weathering which they induce, which leads to a removal of carbon from the atmosphere and a consequent cooling of the atmosphere. It is certainly the case that CO_2 has faithfully followed climatic temperatures through the recent ice ages, and it is difficult not to suppose that it has been a major causative factor in their explanation.

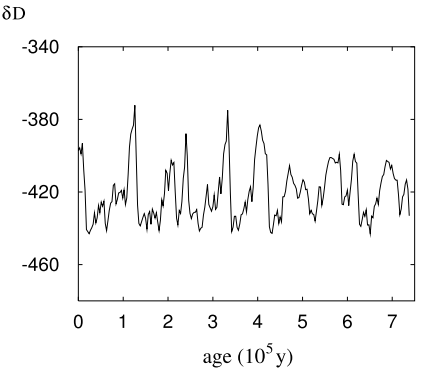

Fig. 2.12 A proxy measurement from deuterium isotope data of the climate of the last 740,000 years. The measurements come from an Antarctic ice core (see the EPICA community members' paper, Agustin et al. (2004), and were provided by Eric Wolff. Each data point is the measurement of deuterium isotope ratios in a column of ice representing 3,000 years accumulation (i.e., the data represent 3,000 year averages). Time moves from right to left along the abscissa, and the deuterium isotope ratio is a proxy measurement of prevailing climatic temperature

If we go further back in time, we encounter much warmer climates. The time of the dinosaurs, extending back to the Triassic, some 200 million years ago, saw a very warm climate and some very large creatures. There were no ice sheets: the Antarctic ice sheet only began to grow some 34 million years ago after the India–Asia collision.

Further back, however, we find evidence of major glaciated periods of Earth history, for example in the Carboniferous period some 300 million years ago. The glacial deposits which indicate this are located in India, South Africa, Australia and South America. But at the time of the glaciation, these continental masses were all sutured together in the great palaeo-continent of Gondwanaland, and they resided at the south pole. The break up of Gondwanaland to form the continents as we now see them only began some 200 million years ago, and is more or less coincident with the global rise in temperature and the flourishing of the dinosauria.

Even earlier in time, we have evidence of further massive glaciation on the supercontinent of Rhodinia during Proterozoic times, some 600 million years ago. The fact that these glaciations occur at then equatorial positions has led to the challenging concept of the 'snowball Earth', the idea that the whole planet was glaciated. Like most outrageous ideas, this is both enticing and controversial; we shall say more about it in Sect. 2.6 below.

2.5.1 Ice-Albedo Feedback

The simplest type of model to explain why ice ages may occur in a sequential fashion is the energy-balance model of Sect. 2.4. On its own, it predicts a stable climatic response to solar radiative input, but when the feedback effect of ice is included, this

alters dramatically. Although simple in concept, the energy-balance model provides the platform for more recent models of 'intermediate complexity'.

The mechanism of the ice-albedo feedback is this. In winter, Antarctica is surrounded by sea ice, and the Arctic ocean is permanently covered by sea ice. Land ice is also present on the Earth near the poles, or in mountainous regions. The presence of ice has a dramatic effect on the surface albedo. While the reflectivity (the fraction of radiation which is reflected) of oceans or forest is typically 0.1, that of sea ice or snow is in the range 0.6–0.8. From Fig. 2.3, we see that 50% of the incoming solar radiation Q (i.e., $0.5Q$) is received at the surface, either directly or through scattering. The albedo of the planet, 0.3, is due to a reflectivity of 0.26 from cloud and atmosphere, and a reflectivity of 0.04 from the surface: since $0.5Q$ reaches the surface, this represents a surface albedo of $0.04/0.5 = 0.08$. However, if the planet were covered in ice, the surface albedo might be 0.7, so that $0.7 \times 0.5 = 0.35$ of the solar radiation would be reflected. Consequently, the planetary albedo would be doubled, from $0.26 + 0.04 = 0.3$, to $0.26 + 0.35 = 0.61$, from this effect alone.

It is thus of interest to examine the effect on the energy-balance equation of including this effect of ice and thus temperature on albedo, since the occurrence of precipitation as snow or rain is essentially related to the atmospheric temperature. We write (2.63) in the form

$$c\dot{T} = R_i - R_o, \tag{2.98}$$

where $c = \rho_a c_p d$ is the specific heat capacity of the atmosphere, and

$$R_i = \frac{1}{4}(1-a)Q, \qquad R_o = \sigma\gamma T^4 \tag{2.99}$$

are, respectively, the incoming short-wave radiation and the emitted IR radiation.

The effect of decreasing temperature on the albedo is to increase the extent of land and sea ice, so that a will increase. It is convenient to define a family of equilibrium albedo functions

$$a_{\mathrm{eq}}(T) = a_1 - \frac{1}{2}a_2\left[1 + \tanh\left(\frac{T - T^*}{\Delta T}\right)\right], \tag{2.100}$$

one example of which is shown in Fig. 2.13. The epithet 'equilibrium' refers to the assumption that the land ice cover is in dynamical equilibrium with the ground surface temperature: more on this below. The effect of the albedo variation on the emitted radiation is shown in Fig. 2.14: R_o is an increasing function of T, but the sigmoidal nature of R_i can lead, for a range of Q and suitable choices of the albedo function, to the existence of multiple steady states. If this is the case, then the equilibrium response diagram for steady states T in terms of Q is as shown in Fig. 2.15.

The parameters used in Fig. 2.14 are chosen to illustrate the multiple intersection of R_i with R_o, but do not correspond to modern climate (for which $T = 288$ K and $R_i = R_o = 235\ \mathrm{W\,m^{-2}}$). The reason is that with more appropriate parameters, such as those used in Fig. 2.15, the two curves become very close, and the range of Q over which multiplicity occurs is very small. Insofar as these parameterisations

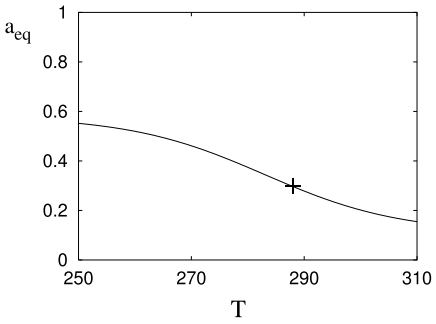

Fig. 2.13 A representation of the possible variation of equilibrium surface albedo $a_{\rm eq}(T)$ due to variations in ice cover due to climatic temperature. The function plotted is $a_{\rm eq}(T)$ given by (2.100), with $a_1 = 0.58$, $a_2 = 0.47$, $T^* = 283$ K, $\Delta T = 24$ K,which tends to 0.58 for small T, and equals 0.3 at about $T = 288$ K (the point marked +)

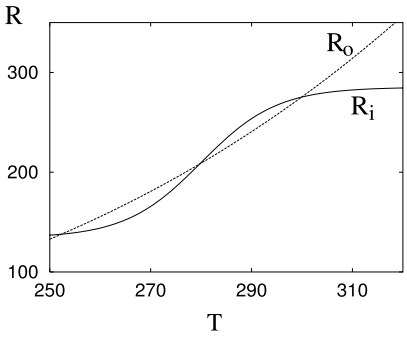

Fig. 2.14 Variation of R_i and R_o with temperature T. Parameters used are $a_1 = 0.6$, $a_2 = 0.45$, $\gamma = 0.6$, $T^* = 280$ K, $\Delta T = 15$ K

apply to the Earth, it does suggest that the current climate is close to a switching point, as seen in Fig. 2.15, corroborating this explanation for ice age formation.

We have seen this kind of S-shaped diagram before in Sect. 1.3.3, where it was used in describing combustion. It is easy to see from Fig. 2.14 that the upper and lower branches in Fig. 2.15 are stable, while the middle branch is unstable; this

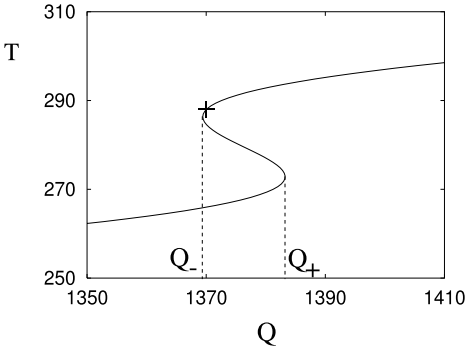

Fig. 2.15 Multivalued response curve for T in terms of Q. Parameters used are $a_1 = 0.58$, $a_2 = 0.47$, $\gamma = 0.6175$, $T^* = 283$ K, $\Delta T = 24$ K. Also shown is the point (+) corresponding to current climate ($Q = 1370$ W m^{-2}, $T = 288$ K)

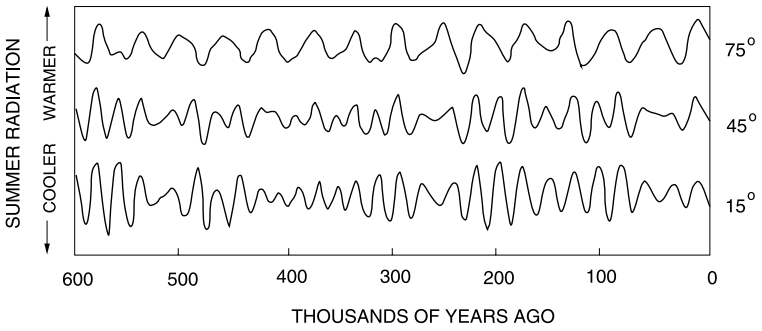

Fig. 2.16 Milankovitch radiation curves for 15° N, 45° N, and 75° N (see Bolshakov 2003). The *lower two curves* indicate the ∼22,000 year precession cycle, while the upper one shows more clearly the 41,000 year tilt cycle

follows because the stability of the equilibria of (2.96) is determined by the slope of $R_i - R_o$ there: if $R_i' < R_o'$, then the equilibrium is stable, and vice versa. Thus if Q varies slowly backwards and forwards beyond Q_- and Q_+, then the temperature will vary up the lower and down the upper branch, with sudden jumps at Q_+ and Q_-. This oscillatory response exhibits *hysteresis*, it is *irreversible*, and it forms the basis for the Milankovitch theory of the ice ages, since the lower branch is associated with widespread glaciation.

2.5.2 The Milankovitch Theory

The solar radiation received seasonally on the Earth is not in fact constant. Due to variations in the Earth's orbit, the value of Q at a point varies by about ±5% either side of its mean. Nor are these variations periodic. Because the solar system has planets (and moons) other than the Earth, and because also the planets do not act exactly as point masses, the orbit of the Earth is not precisely a Keplerian ellipse. The Earth's axis of rotation precesses, its angle of tilt (from the plane of the ecliptic) oscillates, and the eccentricity of the orbit itself oscillates. All of these astronomical features cause the value of Q to oscillate quasi-periodically, when considered for a particular latitude and a particular season. The reason for focussing on a particular season is because of the seasonal imbalance in snowfall, whence it might be supposed that, for example, it is the summer insolation received at (say) 65° N which is important, since this is likely to control the inception of northern latitude ice sheets via year round retention of snow cover and the consequent operation of the ice-albedo feedback. The importance of a particular latitude is due to the fact that the seasonal insolation curves are different at different latitudes, as indeed found by Milankovitch—see Fig. 2.16. The major periodicities in the signals consist of one of 41,000 years due to oscillations in the tilt axis, and periods of 23,000 and 19,000 years in the precessional variation of the rotation axis. The third component,

eccentricity, causes a variation over a period of 100,000 years, though its amplitude is much smaller.

The test of the Milankovitch theory that variations in climate (and thus ice ages) are associated with the variation in Q, can then be made by computing the Fourier power spectrum of a record of past climatic temperature. Oxygen isotope ratios in deep-sea sediment cores (or in ice cores) provide a proxy measurement of temperature, and Fig. 2.12 showed just such a record. When a spectral analysis of records of this type is made, it is indeed found that the principal frequencies are (in order of decreasing amplitude) 100 ka (100,000 years), 41, 23 and 19 ka. This seems to serve as dramatic confirmation of the Milankovitch theory. In our simple energy-balance model, the concept is enunciated by the hysteretic oscillations exhibited by the system as Q varies.

2.5.3 Nonlinear Oscillations

There is currently a consensus that the Milankovitch orbital variation indeed acts as pacemaker for the Quaternary ice ages, but it is as well to point out that there is an essential problem with the Milankovitch theory, even if the basis of the concept is valid. The spectral insolation frequencies do match those of the proxy climate record, with one essential discrepancy: the largest climatic signal is the 100 ka period. Ice ages essentially last 90 ka, with an interval of 10 ka between (and since the last ice age terminated about 10 ka ago, as the Scottish ice sheet withdrew from the lochs in the Highlands, and the North American Laurentide ice sheet shrank from the Great Lakes, we might be on the verge of starting the next). But the 100 ka astronomical signal is very weak, and it is unrealistic to imagine that the forcing can directly drive the strong response which is observed. What may happen is that the weak 100 ka forcing *resonates* with the climatic system, suggesting that the climate is essentially a (nonlinear) oscillator, with a natural period close to 100 ka, which is tuned by the astronomical forcing. A mathematical paradigm would be the forced Van der Pol oscillator

$$\ddot{x} + \varepsilon\left(x^2 - 1\right)\dot{x} + \omega^2 x = f(t), \tag{2.101}$$

where $f(t)$ would represent the astronomical forcing. If ε is small, the oscillator has a natural frequency close to $2\pi/\omega$, and if forced by a frequency close to this, tuning can occur. If the oscillator is nonlinear, other exotic effects can occur: subharmonics, chaos; no doubt these effects are present in the forced climate system too.

The simplest kind of model which can behave in an oscillatory manner is the energy-balance model (2.98) subjected to an oscillating radiation input which can drive the climate back and forth between the cold and warm branches, presumably representing the glacial and interglacial periods. Two questions then arise; where does the 100,000 year time scale come from, and why is the climatic evolution through an ice age (slow development, rapid termination) so nonlinear?

There are three principal components of the climate system which change over very different time scales. These are the atmosphere, the oceans and the ice sheets. The time scale of response of ice sheets is the longest of these, and is measured by l/u, where l is a horizontal length scale and u is a horizontal velocity scale. Estimates of $l \sim 1000$ km and $u \sim 100$ m y^{-1} suggest a time scale of 10^4 y, which is within range of the value we seek. Since ice sheet extent is directly associated with albedo. it suggests that a first realistic modification of the energy-balance model is to allow the ice sheets, and therefore also the albedo, to respond to a changing temperature over the slow ice sheet time scale t_i. A simple model to do this is to write

$$\begin{aligned} c\dot{T} &= \frac{1}{4}Q(1-a) - \sigma\gamma T^4, \\ t_i\dot{a} &= a_{\text{eq}}(T) - a, \end{aligned} \tag{2.102}$$

and $a_{\text{eq}}(T)$ is the equilibrium albedo represented in Fig. 2.13. Since the thermal response time scale is so rapid (months), we may take the temperature to be the equilibrium temperature,

$$T = T(a, Q) = \left[\frac{Q(1-a)}{4\sigma\gamma}\right]^{1/4}. \tag{2.103}$$

The energy-balance model thus reduces to the first order albedo evolution equation

$$t_i\dot{a} = I(a, Q) - a, \tag{2.104}$$

where

$$I(a, Q) = a_{\text{eq}}\big[T(a, Q)\big]. \tag{2.105}$$

As Q varies backwards and forwards about the critical switching values in Fig. 2.15, the ice extent (as indicated by a) changes on the slow time scale t_i, aiming to follow the hysteretically switching equilibria. Oscillatory inputs Q do indeed cause oscillations; if t_i is sufficiently small, these are large scale, going from warm branch to cold branch and back, whereas at larger t_i, two different oscillatory climates are possible, a cold one and a warm one (see Question 2.14). None of these solutions bears much resemblance to real Quaternary ice ages, for which a more sophisticated physical model is necessary.

2.5.4 Heinrich Events

The study of climate is going through some exciting times. The pulse of the ice ages can be seen in Fig. 2.12, but the signal appears noisy, with numerous irregular jumps. Twenty or thirty years ago, one might have been happy to ascribe these to the influence of different spectral components of the Milankovitch radiation curves on a nonlinear climatic oscillator, together with a vague reference to 'noisy' data.

Increasingly in such circumstances, however, one can adopt a different view: what you see is what you get. In other words, sharp fluctuations in apparently noisy data are actually signals of real events. Put another way, noise simply refers to the parts of the signal one does not understand.

It has become clear that there are significant climate components which cause short term variations, and that these events are written in the data which are exhumed from ocean sediment cores and ice cores. Perhaps the most dramatic of these are *Heinrich events*. Sediment cores retrieved from the ocean floor of the North Atlantic reveal, among the common ocean sediments and muds, a series of layers (seven in all have been identified) in which there is a high proportion of lithic fragments. These fragments represent ice rafted debris, and are composed of carbonate mudstones, whose origin has been identified as Hudson Bay. The spacing between the layers is such that the periods between the Heinrich events are 5,000–10,000 years.

What the Heinrich events are telling us is that every 10,000 years or so (more or less periodically) during the last ice age, there were episodes of dramatically increased iceberg production, and that the ice in these icebergs originated from the Hudson Bay underlying the central part of the Laurentide ice sheet. Ice from this region drained through an ice stream some 200 km wide which flowed along the Hudson Strait and into the Labrador sea west of Greenland.

The generally accepted cause of these events is also the most obvious, but equally the most exciting. The time scale of 10,000 years is that associated with the growth of ice sheets (for example, by accumulation of 0.2 $\mathrm{m\,y^{-1}}$ and depth of 2000 m), and so the suggestion is that Heinrich events occur through a periodic surging of the ice in the Hudson Strait, which then draws down the Hudson Bay ice dome. This would sound like a capricious explanation, were it not for the fact that many glaciers are known to surge in a similar fashion; we shall discuss the mechanism for surging in Chap. 10.

Another feature of Heinrich events is that they appear to be followed by sudden dramatic warmings of the Earth's climate, which occur several hundred years after the Heinrich event. Dating of these can be difficult, because dating of ice cores and also of sediment cores sometimes requires an assumption of accumulation or sedimentation rates, so that precise association of timings in different such cores can be risky.

How would Heinrich events affect climate? There are two obvious ways. A sudden change in an ice sheet elevation might be expected to alter storm tracks and precipitation patterns. Perhaps more importantly, the blanketing of the North Atlantic with icebergs is likely to affect oceanic circulation. Just like the atmosphere, the ocean circulation is driven by horizontal buoyancy induced by the difference between equatorial and polar heating rates. This large scale flow is called the global thermohaline circulation, and its presence in the North Atlantic is the cause of the gulf stream (see also Sect. 3.9), which promotes the temperate climate of Northern Europe, because of the poleward energy flux it carries. If this circulation is disrupted, there is liable to be an immediate effect on climate.

If the North Atlantic is covered by ice, one immediate effect is a surface cooling, because of the increased albedo. This is liable to cause an increase in the thermohaline circulation, but would not cause atmospheric warming until the sea ice melted.

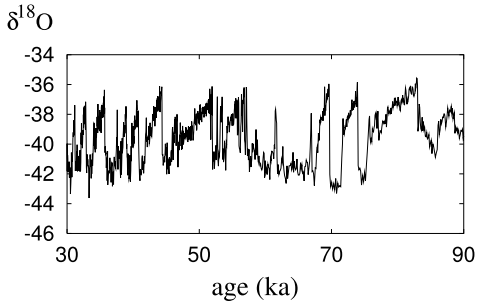

Fig. 2.17 Oxygen isotope ratio (δ^{18}O) measurements from the GRIP ice core on Greenland, as a function of age in ka (1 ka = 1000 years). This is a proxy for surface temperature (with four units corresponding to about 10 K on the vertical axis). The data represent averages from segments of 55 cm length, and the age scale is determined from a model of ice burial rate. Near the surface, the separate measurements are two-to-three yearly, but the compression of ice with burial causes the ice segments to encompass longer and longer time periods. At the age of 90,000 years ago (at a depth of some 2685 m), each segment is a time average of some 120 years. Thus the data are increasingly sparsely resolved further into the past

On the other hand, the melting itself releases fresh water, which is buoyant in a saline ocean, suggesting a shutdown of ocean circulation. As we discuss further below, this can lead, following a delay, to a massive restart of ocean circulation and thus sudden warming.

2.5.5 Dansgaard–Oeschger Events

There are other rapid changes in the climate which are seen during the last ice age. Figure 2.17 shows a segment of oxygen isotope measurements (a proxy for surface temperature) from the GRIP ice core on Greenland. Time marches from right to left on this diagram. There are numerous sudden rises in temperature that can be seen, followed by a more gentle sinking of temperature. These sharp rises are called *Dansgaard–Oeschger events*. Between 30,000 and 45,000 years B. P., for example there are seven of these events, thus, like Heinrich events, they occur at reasonably regular intervals, with a typical repetition period being in the region of about 1,500 years. The association of the D–O events with oceanic salt oscillations is described by Schmidt et al. (2006), for example.

Let us examine one of these events in greater detail: that of the D–O event between 44,000 and 45,000 years B. P. In the GRIP core, this ice lies between 2,316 and 2,330 metres depth. A higher resolution data set is that of Sigfus Johnsen, and is shown in Fig. 2.18. This shows that the climatic temperature changes abruptly, over a time scale of about a century. Other such inspections show that the transitions can be even shorter.

What is the cause of these warming events? Why are they so rapid, and why do they have a regular period of some 1,500 years? The idea here is that the climate

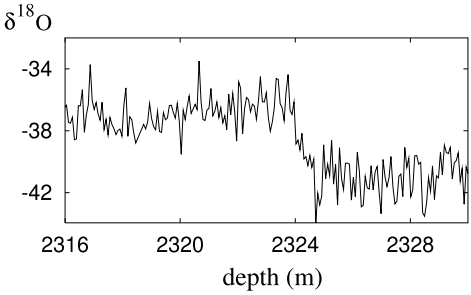

Fig. 2.18 GRIP core data between 2,316 m and 2,330 m. The sharp jump near 2,324 m occurs over a range of about 1.3 metres, corresponding to a time interval of some 90 years

in the northern hemisphere is essentially controlled by the oceanic conveyor circulation, and so the change in climate occurs because of a sudden disruption to this. Model studies have shown that an injection of a massive pulse of fresh water into the North Atlantic can cause just such a disruption.[8]

The mechanism is, however, counter-intuitive. A warm climate is associated with a vigorous circulation, and a cold one with the circulation off, but a freshwater pulse has the initial effect, being buoyant, of switching the (relatively weak) circulation off. This causes a climatic cooling. However, the cooling is temporary, because a situation with no circulation is unstable. When convection begins again, it does so dramatically, with deep water formation occurring further north (as it does in interglacial times), causing a sudden shift to a warmer climate. The same model studies have shown that even larger meltwater pulses, such as would occur following the melting induced by large scale iceberg production, can lead, after the initial cooling of the north Atlantic, to a subsequent extreme warming comparable to that seen following Heinrich events.

If freshwater pulses are the cause of the sudden climate shifts, what is their origin? For Heinrich events, the ice rafted debris gives the clue; for Dansgaard–Oeschger events, there is apparently no such clue. However, it is pertinent to note that these events are associated with the presence of large ice sheets. If we seek an explanation by means of freshwater pulses, then the most obvious (and really, the only) candidate for the source of the pulses is that they come from meltwater from the ice, and one way in which meltwater drainage is known to occur episodically is in the large sub-glacial floods known as jökulhlaups. As with surges, these are well documented from beneath glaciers. It has been less common to imagine that they could occur from beneath modern day ice sheets, but in fact such floods are being increasingly observed to happen below the Antarctic Ice Sheet. As a hypothesis it seems sensible to suggest that Dansgaard–Oeschger events might arise as a consequence of semi-regular Laurentide jökulhlaups which occur with a rough periodicity of one to two thousand years. The question then arises as to whether such floods are dynamically possible, and whether they could produce the necessary fresh water at the required frequency to do the job. We shall re-examine this question in Chap. 11.

[8]This is not the only possible mechanism. Another is the North Atlantic salt oscillator, discussed in Sect. 2.5.7.

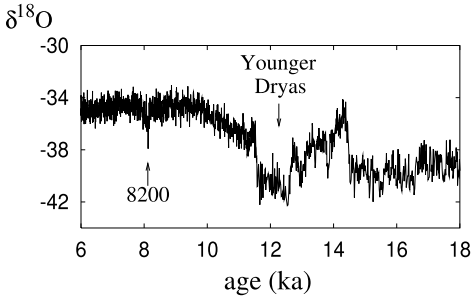

Fig. 2.19 Oxygen isotope data from the GRIP core at the transition to the Holocene interglacial

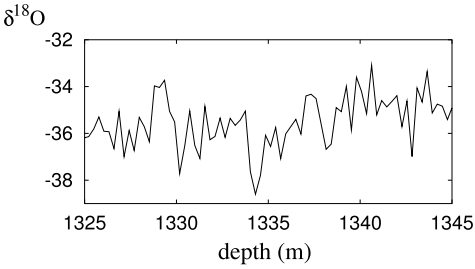

Fig. 2.20 High resolution data set from 20 metres of ice near the 8,200 year event

2.5.6 The 8,200 Year Cooling Event

One climatic event which is thought to have been caused by a sub-glacial flood is a sudden cooling event dated to 8,200 years B. P. This is shown in context in Fig. 2.19. which also shows the termination of the ice age after the Younger Dryas readvance of the ice sheets between 13,000 and 11,600 years B. P. Two Heinrich events precede the two warmings at about 15,000 and 12,000 years B. P. Following the Younger Dryas, there is a gradual return to an interglacial climate by 9,500 years B. P., and the onset of the current (Holocene) period. A cursory glance might suggest that the 8,200 year dip is just a noisy outlier, but this is not the case. It represents a genuine climatic cooling of some 4 K.

Figure 2.19 shows a high resolution record of this event. Inspection of the coarse (55 cm samples) GRIP data shows that the 8,200 year event is actually (on the age scale used) at 8,126 years B. P., and occurs in a single 55 cm segment at a depth of 1334 metres; blink, and you miss it. At this depth, six metres of ice (1,331–1,337) is considered to represent 65 years of accumulation. Plotting the data using Johnsen's higher resolution data set over a more restricted range, we can see (Fig. 2.20) various features.

One is that the event occupies three data points from an ice depth between 1,334 and 1,335 metres depth. These three samples are 27.5 cm long, as are the two immediately above and below. This suggests that the 'duration' of the event is between 82 and 137 cm, which corresponds to a period of between 9 and 15 years. This is incredibly fast.

The other thing to notice from Fig. 2.20 is that there are a good number of other large spikes and oscillations. Since, more or less, each data point represents a three

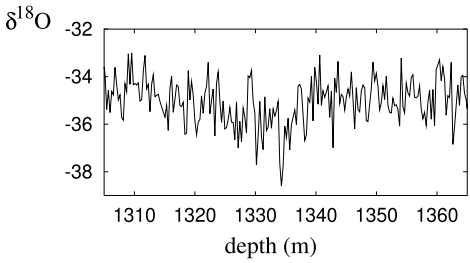

Fig. 2.21 The cooling trend of the 8,200 year event

year average, these are not seasonal fluctuations. Do they represent real events, or simply the natural fluctuation of the climate from year to year? If one looks at a slightly larger slice of the time series, from 1305 m to 1365 m, it is apparent (see Fig. 2.21) that these short term fluctuations sit on top of a broader cooling trend from about 1340 to 1315 m, with rapid decrease in the first 5 m (∼54 years), and slower recovery over the following 20 m (∼217 years). It is perhaps easier to imagine that this slower average trend represents the underlying event.

The explanation which is currently thought to apply to this event is that it is caused by a sub-glacial jökulhlaup which drains the massive proglacial Lake Agassiz into the Hudson Strait, whence it pours into the Labrador Sea and the North Atlantic. As the remnant of the Laurentide ice sheet dwindles, it builds up a massive proglacial lake on its southern margin. The topography is such that this lake is prevented from outflow to the south, and at some point it drains catastrophically, either over or more probably under the ice sheet to the north. The resulting fresh water efflux to the North Atlantic causes the cooling event.

One might wonder, if glacial meltwater pulses cause convective shutdown, cooling, and then subsequent warming, why would an interglacial one produce only the cooling? The putative answer to this lies in our idea of what a meltwater pulse will actually do. In an interglacial climate, the ocean circulation is strong, and meltwater weakens it temporarily: a cooling. In a glacial climate, the circulation is weaker, and deep water formation occurs further south, say near Iceland, than it does currently. Then a meltwater pulse may shut down the circulation entirely, which would indeed cause further cooling, but the resultant overshoot when circulation resumes causes the warming. Since Dansgaard–Oeschger events occur at the end of cooling cycles, the initial cooling is swamped by the trend. It is interesting to note that the D–O warming events in Fig. 2.19 are initiated at 14,500 B. P. and 11,600 B. P., the interval between these being 2,900 years. The interval between the Younger Dryas and the 8,200 event is about 3,500 years. If the D–O events are due to sub-glacial floods, then possibly the 8,200 event is simply the last of these. It is then tempting to look further on for similar, smaller events. There is one at 5,930 B. P., for example, and another at 5,770 B. P.; these are about another 2,400 years further on. It is a natural consequence of the hypothesis that jökulhlaups occurred from below the Laurentide ice sheet to suppose that they will occur also from beneath Greenland and Antarctica, and that this may continue to the present day. It has been suggested, for instance, that the cool period in Europe between 1550 A. D. and 1900 was due to a similar upset of the oceanic circulation.

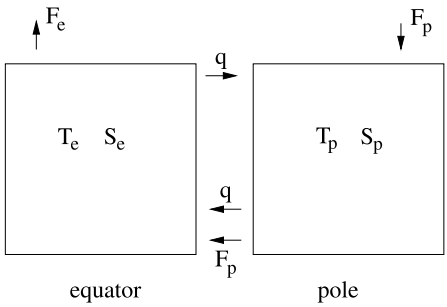

Fig. 2.22 Stommel's box model of the North Atlantic circulation

2.5.7 North Atlantic Salt Oscillator

Deeply embroiled in this whole saga of Quaternary climate and the ice ages is the rôle of the North Atlantic ocean circulation. For the descriptions we have given of Heinrich events and Dansgaard–Oeschger events to work, the ocean needs to be able to circulate in different ways. That this is indeed the case has been found in a number of model studies, and the resultant flip-flop circulation is sometimes known as the 'bipolar seesaw'. In its original form, the idea is due to Henry Stommel, and can be described with a simple 'box' model, as illustrated in Fig. 2.22.

In this model, we parameterise the thermohaline circulation in the North Atlantic by considering it to be partitioned between two compartments, an equatorial and a polar one. We label the temperature T, salinity (mass fraction of salt) S, density ρ and volume V of each box by a suffix 'e' or 'p', and we write conservation laws of mass, energy and solute, and an equation of state, for each box. Transports in and out of each box are considered to be a freshwater flux F_p to the polar cell, an evaporative flux F_e from the equatorial cell, and a convective flux q due to buoyancy difference from equatorial to polar cell. (The reverse flux is then $q + F_p$ in order to allow conservation of the sizes of both cells.)

Suitable equations to describe the convective flow are then

$$\begin{aligned}
\frac{d}{dt}(\rho_e c V_e T_e) &= A_e H_e + \rho_p c T_p \big(F_p + |q|\big) - \rho_e c T_e |q|, \\
\frac{d}{dt}(\rho_p c V_p T_p) &= A_p H_p - \rho_p c T_p \big(F_p + |q|\big) + \rho_e c T_e |q|, \\
\frac{d}{dt}(\rho_e V_e S_e) &= -\rho_e |q| S_e + \rho_p S_p \big(F_p + |q|\big), \\
\frac{d}{dt}(\rho_p V_p S_p) &= \rho_e |q| S_e - \rho_p S_p \big(F_p + |q|\big), \\
\frac{d}{dt}\big[\rho_e V_e (1 - S_e)\big] &= \rho_p^0 F_p - \rho_e F_e, \\
\frac{d}{dt}\big[\rho_p V_p (1 - S_p)\big] &= 0,
\end{aligned} \tag{2.106}$$

$$\rho_e = \rho_0\big[1 - \alpha(T_e - T_0) + \beta(S_e - S_0)\big],$$
$$\rho_p = \rho_0\big[1 - \alpha(T_p - T_0) + \beta(S_p - S_0)\big],$$
$$q = k(\rho_e - \rho_p).$$

The terms in these equations are fairly self-explanatory. α and β are coefficients of thermal and saline expansion, ρ_p^0 is the freshwater density, A_e and A_p are the equatorial and polar ocean surface areas, and for simplicity we take $A_p = A_e = A$. The heating terms H represent the heat flux to the deep ocean from the surface waters. The sea surface temperature is determined by a radiative balance, which determines equatorial and polar surface temperatures T_e^0 and T_p^0, say. We then suppose that heat transfer to the deep ocean can be parameterised by a suitable heat transfer coefficient h_T, thus we put

$$H_e = h_T\big(T_e^0 - T_e\big), \qquad H_p = h_T\big(T_p^0 - T_p\big). \tag{2.107}$$

If we add the two energy equations, we have

$$\frac{d}{dt}(\rho_e c V_e T_e + \rho_p c V_p T_p) = h_T A\big(T_e^0 + T_p^0 - T_e - T_p\big). \tag{2.108}$$

We use the facts that $\rho_{e,p} \approx \rho_0$ and we will suppose that V_e and V_p, both approximately constant, are also approximately equal, $V_{e,p} \approx V_0$. It then follows from (2.108) that, after an initial transient,

$$T_e + T_p \approx T_e^0 + T_p^0, \tag{2.109}$$

and we suppose this generally to be the case. We define V_0 by

$$\rho_e V_e T_e + \rho_p V_p T_p = 2\rho_0 V_0 T_0, \tag{2.110}$$

where

$$T_0 = \frac{1}{2}\big(T_e^0 + T_p^0\big), \tag{2.111}$$

and we then define the temperature excess T via

$$T_e = T_0 + T, \qquad T_p = T_0 - T. \tag{2.112}$$

If we now make the assumptions that $\rho_e \approx \rho_0$, $V_e \approx V_0$ in $(2.106)_1$, then we have the approximate equation for T:

$$\rho_0 c V_0 \dot{T} = \frac{1}{2}\big[h_T A\big(T_e^0 - T_p^0\big) + \rho_0 c F_p\big(T_e^0 + T_p^0\big)\big] - \big(h_T A + \rho_0 c F_p + 2\rho_0 c|q|\big)T. \tag{2.113}$$

In a similar way, we have

$$\rho_e V_e S_e + \rho_p V_p S_p = 2\rho_0 V_0 S_0, \tag{2.114}$$

where S_0 is constant, and we define

$$S_e = S_0 + S, \qquad S_p = S_0 - S. \tag{2.115}$$

With the same Boussinesq type assumption, that $\rho_e \approx \rho_0$ and $V_e \approx V_0$, we obtain

$$V_0 \dot{S} = F_p S_0 - \big(F_p + 2|q|\big)S. \tag{2.116}$$

Equations (2.113) and (2.116) are essentially Stommel's box model. Their validity relies on the use of the other equations to show that it is indeed realistic to take ρ and V as constant, though these assumptions appear fairly reasonable ones. Note that with the definitions of the variables, we have

$$q = 2k\rho_0(-\alpha T + \beta S). \tag{2.117}$$

To parameterise the heat transfer coefficient h_T, we use the ideas of Reynolds averaging for turbulent flow (see Appendix B). This suggests choosing

$$h_T = \frac{\varepsilon_T \rho_0 c q_0}{A}, \tag{2.118}$$

where the number ε_T is typically chosen to be in the range 0.001–0.01, and q_0 is a suitable scale for q, defined below in (2.124).

We non-dimensionalise the box model by writing

$$T = \Delta T\, \theta, \qquad S = \Delta S\, s, \qquad t \sim t_0, \qquad q \sim q_0, \tag{2.119}$$

where we choose

$$\Delta T = \frac{1}{4}\left[\varepsilon_T\big(T_e^0 - T_p^0\big) + \frac{F_p}{q_0}\big(T_e^0 + T_p^0\big)\right], \qquad \Delta S = \frac{F_p S_0}{2q_0}, \qquad t_0 = \frac{V_0}{2q_0}. \tag{2.120}$$

Using the values in Table 2.1, we find $\Delta T \approx 1$ K, $\Delta S \approx 1.1 \times 10^{-4}$, $t_0 \approx 150$ y. We use a value of q_0 as observed, rather than k, which we would in any case choose in order that q was the right size, some 16 Sv (Sverdrups: 1 Sv $= 10^6$ m^3 s^{-1}).

The observed surface temperature variation is of order 30 K, and the observed surface salinity variation is of order 30×10^{-4}. However, these values represent the concentrative effect of surface evaporation and heating; at depth (as is more relevant) the variations are much smaller, of order 2 K for temperature and 4×10^{-4} for salinity at 1000 m depth. The time scale is comparable to the time scales over which Dansgaard–Oeschger events occur. These features suggest that this simple model has the ring of truth.

We can write the model in dimensionless form as

$$\begin{aligned} \dot{\theta} &= 1 - \big(\mu + |q|\big)\theta, \\ \dot{s} &= 1 - \big(\varepsilon + |q|\big)s, \\ q &= \kappa(-\theta + Rs), \end{aligned} \tag{2.121}$$

Table 2.1 Typical parameter values for the Stommel box model

Parameter	Value
ρ_0	10^3 kg m^{-3}
c	4.2×10^3 J kg^{-1} K^{-1}
V_0	1.6×10^{17} m^3
A	0.4×10^{14} m^2
ε_T	0.01
T_e^0	300 K
T_p^0	270 K
T_0	285 K
F_p	10^5 m^3 s^{-1}
q_0	1.6×10^7 m^3 s^{-1}
α	1.8×10^{-4} K^{-1}
β	0.8
S_0	0.035

where the parameters are given by

$$\begin{aligned} \varepsilon &= \frac{F_p}{2q_0}, \qquad \mu = \frac{1}{2}\left(\varepsilon_T + \frac{F_p}{q_0}\right), \\ R &= \frac{\beta \Delta S}{\alpha \Delta T}, \qquad \kappa = \frac{2k\rho_0 \alpha \Delta T}{q_0}. \end{aligned} \tag{2.122}$$

Typical values of these are, from Table 2.1,

$$\varepsilon \sim 0.003, \qquad \mu \sim 0.005, \qquad R \sim 0.5, \tag{2.123}$$

and we can assume without loss of generality that $\kappa = 1$, which fixes the value of q_0 (given k):

$$q_0 = 2k\rho_0 \alpha \Delta T. \tag{2.124}$$

Both ε and μ are small, and we will take advantage of this below.

It is straightforward to analyse (2.121) in the phase plane. Figure 2.23 shows the steady states of q as a function of R when $\mu = 0.005$, $\varepsilon = 0.003$. Neglecting ε and taking μ to be small, we deduce that the steady states are given by

$$\begin{aligned} q &\approx (R-1)^{1/2}, \quad R > 1, \\ q &\approx -(1-R)^{1/2}, \quad R < 1, \end{aligned} \tag{2.125}$$

if $q = O(1)$, and

$$q \approx \pm \frac{\mu R}{1-R}, \quad R < 1, \tag{2.126}$$

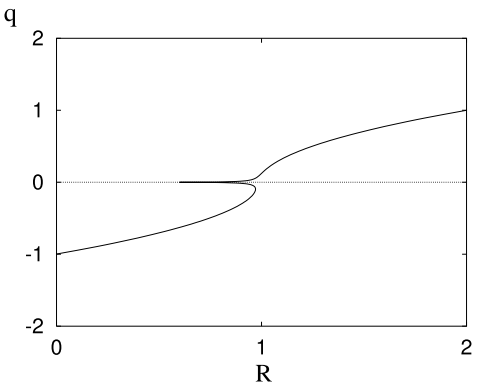

Fig. 2.23 Steady states of (2.125) as a function of R

if $q = O(\mu)$. As we might expect, the upper and lower branches are stable, and the middle one is unstable. The upper branch corresponds to present climate, with a northwards circulation at the surface. The stable lower branch corresponds to a reversed haline circulation (thermal buoyancy dominates saline buoyancy because $R < 1$).

Stommel's box model is not an oscillator as such, but it does point out the possibility of multiple convective states of the North Atlantic, and this feature has been found to be robust in other models. What appears to distinguish more realistic models from the Stommel box model is that they allow North Atlantic deep water formation to occur at different latitudes. Thus rather than simply switching from a northerly flow to a southerly one, adjustments can occur between strong northerly flows with deep water formation in the Norwegian sea, and weaker flows with deep water formation further south. It seems that these switches are instrumental in causing the rapid climatic changes during ice ages.

2.6 Snowball Earth

The story of climate on the Earth becomes perhaps more fascinating if we shift our gaze from the relatively recent geologic past to that of more ancient times. There is evidence of glaciation on Earth throughout geologic time, and on all continents. Since the continents move, through the process of plate tectonics, on time scales of hundreds of millions of years, and since their positions and configuration are instrumental in determining ocean circulations and carbon budget (as described below), it seems that plate tectonics is implicated in the long term control of climate.

Recently, one of these periods of glaciation has been at the centre of a scientific controversy concerning what has been picturesquely termed the 'snowball Earth'. In the Neoproterozoic era, between about 750 and 550 million years ago, there was a sequence of glacial episodes. At that time, the Earth's land masses were assembled into a supercontinent called Rodinia, which broke up in a similar way to that

in which Gondwanaland fragmented some 200 million years ago.[9] The glaciation of Rodinia would not in itself be surprising, except for the fact that it seems that the supercontinent was located near the equator. It is not impossible for glaciers to exist in equatorial regions at high altitudes (there is an ice cap today on Mount Kilimanjaro in Tanzania), but the suggestion for the Neoproterozoic is that there were widespread ice sheets, and that in fact the land masses were covered with ice. If we suppose also that the oceans were largely ice covered, we see how the concept of a snowball Earth arises.

Although the concept of an ice-covered Earth is entirely consistent with a simple energy-balance model, it is less easy to explain in detail. At that period, the Sun was 6% fainter than today. Model simulations appear able to produce equatorial glaciation providing there is very little CO_2 in the atmosphere, but it is not obvious how to produce such low levels. Nor is it easy to see how to terminate a snowball glaciation.

An interesting idea to explain this latter conundrum is the widespread occurrence of cap carbonate rocks overlying the glacigenic tillites formed from the sub-glacial basal sediments. The idea is that with widespread glaciation and very low temperatures, there would be no water vapour in the atmosphere. Subglacial volcanic eruptions would continue to produce CO_2 however, and with no clouds or water vapour to dissolve it (and rain it out), it would simply build up in the atmosphere. Eventually, the consequent greenhouse effect would cause a rise in temperature, followed by massive deglaciation, moistening of the atmosphere, and thus widespread acid rain. The resulting weathering processes produce the cap carbonate rocks which are seen overlying the glacial tillites.

If this end part of the story is enticing, it is not easy to initiate an equatorial glaciation. One possible way is to allow increased weathering of an equatorial supercontinent (because of tropical climate) which causes reduction of atmospheric CO_2; this then causes the cooling which initiates the glaciation. Once under way, the ice-albedo feedback effect leads to the snowball. Evidently, the whole account relies strongly on the interaction of the carbon cycle with climate. This idea is attractive, because it is widely thought that the onset of the current ice age climate originated with the collision of India and Asia some fifty million years ago. The resulting (and continuing) uplift of the Himalayas resulted in massively increased weathering rates, and therefore reduction of atmospheric CO_2 and consequent planetary cooling. It is thought that the initial growth of the Antarctic Ice Sheet some 34 million years ago is a consequence of this cooling.

2.6.1 The Carbon Cycle

Just as living organisms have a variety of cycles (sleep-wake cycle, menstrual cycle, cell renewal and so on), so the Earth has a number of cycles. Water, rock, topography

[9] The problems of plate tectonics are discussed in Chap. 8.

all go through cycles, which we will describe later in this book. There is also a carbon cycle, which we now describe, which is central to plant and animal life, and is also central to the long term control of the Earth's temperature. We have only to look at what has happened on Mars and Venus to see how delicate the control of climate is.

Carbon dioxide is produced as a by-product of volcanism. When mantle rocks melt, some CO_2 is dissolved in the melt, and depressurisation of the ascending magma causes exsolution. This eruptive production adds about 3×10^{11} kg y^{-1} to the atmosphere. On the Earth, water in the atmosphere dissolves the CO_2, forming a weak carbonic acid, and thus when rain falls, it slowly dissolves the silicate rocks of the continental crust. This process is called weathering. One typical reaction describing this dissolution is

$$CaSiO_3 + 2CO_2 + H_2O \longrightarrow Ca^{2+} + 2HCO_3^- + SiO_2 : \tag{2.127}$$

water dissolves calcium silicate (wollastonite) in the presence of carbon dioxide to form calcium ions, bicarbonate ions and silica. A similar reaction produces magnesium ions.

The ionic species thus produced run off in streams and rivers to the oceans, where the further reaction

$$Ca^{2+} + 2HCO_3^- \longrightarrow CaCO_3 + CO_2 + H_2O \tag{2.128}$$

creates carbonate sediments. These sink to the ocean floor where they are eventually subducted back into the Earth's mantle. Overall, the pair of reactions (2.127) and (2.128) can be summed to represent

$$CaSiO_3 + CO_2 \longrightarrow CaCO_3 + SiO_2. \tag{2.129}$$

A very simple model to describe the evolution of the atmospheric CO_2 concentration is then

$$\dot{m}_{CO_2} = -A_L W + v_{CO_2}, \tag{2.130}$$

where m_{CO_2} is the mass of CO_2 in the atmosphere, A_L is the available land surface for weathering, W is the rate of weathering, and v_{CO_2} is the eruptive production rate of CO_2. It is common practice in discussing CO_2 levels to measure the amount of CO_2 as a pressure, i.e., in bars. The conversion is done by defining the partial pressure of CO_2 as

$$p_{CO_2} = \frac{m_{CO_2} g M_a}{A M_{CO_2}}, \tag{2.131}$$

where g is gravity, A is total planetary surface area, and M_a and M_{CO_2} are the molecular weights of air and CO_2, respectively. The argument for this is the following. If m_a is the atmospheric mass (of air), then m_a/M_a is the number of moles of air in the atmosphere, while m_{CO_2}/M_{CO_2} is the number of moles of CO_2 in the

atmosphere. Then Dalton's law of partial pressures states that

$$\frac{p_{CO_2}}{p_a} = \frac{m_{CO_2} M_a}{M_{CO_2} m_a}, \tag{2.132}$$

and also the atmospheric air pressure p_a is given by

$$p_a = \frac{m_a g}{A}. \tag{2.133}$$

The current atmospheric carbon mass is around 750 Gt (gigatonnes, 10^{12} kg). Multiplying by the ratio 44/12 of the molecular weights of carbon dioxide and carbon yields the current value of $m_{CO_2} \approx 2.75 \times 10^{15}$ kg. Using $g = 9.81\ \mathrm{m\,s^{-2}}$, $A = 5.1 \times 10^{14}\ \mathrm{m^2}$, $M_a = 28.8 \times 10^{-3}\ \mathrm{kg\,mole^{-1}}$, $M_{CO_2} = 44 \times 10^{-3}\ \mathrm{kg\,mole^{-1}}$, this converts to a value of $p_{CO_2} = p_0 = 0.35 \times 10^{-3}$ bars, or 35 Pa. In fact, the actual partial pressure of CO_2 in the atmosphere in 2000 was about 36 Pa, or 360 μatm, or 370 ppmv (parts per million by volume) of dry air. It is the latter figure which is commonly reported, and it continues to rise relentlessly.

Weathering Rate

In general we may suppose that $W = W(p_{CO_2}, T, r)$, where T is temperature and r is runoff rate of water to the oceans. This dependence encapsulates the reaction rate of (2.129), and the rate of product removal by runoff. Weathering rates have been measured and range from $0.25 \times 10^{-3}\ \mathrm{kg\,m^{-2}\,y^{-1}}$ in arid regions to $16 \times 10^{-3}\ \mathrm{kg\,m^{-2}\,y^{-1}}$ in the tropics.[10] If we suppose that (2.130) applies in equilibrium, then the consequent current average value would be $W_0 \approx 2.2 \times 10^{-3}\ \mathrm{kg(CO_2)\,m^{-2}\,y^{-1}}$, which appears reasonable. This uses values of $A_L = 1.5 \times 10^{14}\ \mathrm{m^2}$ and volcanic production rate $v_{CO_2} = 3.3 \times 10^{11}\ \mathrm{kg\,y^{-1}}$.[11]

One relation which has been used to represent weathering data is

$$W = W_0 \left(\frac{p_{CO_2}}{p_0} \right)^{\mu} \exp\left[\frac{T - T_0}{\Delta T_c} \right], \tag{2.134}$$

where $\mu = 0.3$, and the subscript zero represents present day values: thus $T_0 \approx 288$ K, as well as the values of p_0 and W_0 given above. The current value of the

[10] The units here are in terms of silica, SiO_2. If we suppose that weathering is described by the reaction (2.129), then one mole of CO_2 (of weight 44 grams) is used to produce one mole of SiO_2 (of weight 60 grams). So to convert units of $\mathrm{kg(SiO_2)\,m^{-2}\,y^{-1}}$ to units of $\mathrm{kg(CO_2)\,m^{-2}\,y^{-1}}$, multiply by $44/60 \approx 0.73$.

[11] The current *net* annual addition of CO_2 to the atmosphere because of fossil fuel consumption and deforestation is about 3.5 Gt carbon, or $1.3 \times 10^{13}\ \mathrm{kgCO_2\,y^{-1}}$; this is forty times larger than the volcanic production rate. (The actual rate of addition is more than twice as large again, but is compensated by net absorption by the oceans and in photosynthesis.)

Earth's runoff is $r_0 \approx 4 \times 10^{13}$ m^3 y^{-1}, and in general runoff will depend on temperature (by equating runoff to precipitation to evaporation). This dependence is subsumed into the exponential in (2.134). In general, $\partial W/\partial p_{CO_2} > 0$, so that with constant production rate, CO_2 will reach a stable steady state. An inference would be that dramatic variations of climate and CO_2 levels in the past have been due to varying degrees of volcanism or precipitation on altered continental configurations, associated with long time scale plate tectonic processes.

Energy Balance

In seeking to describe how climate may depend on the carbon cycle, we use an energy-balance model. Thus, we combine the ice sheet/energy-balance model (2.102) with (2.130), to find the coupled system for T, a and p_{CO_2}:

$$\begin{aligned} c\dot{T} &= \frac{1}{4}Q(1-a) - \sigma\gamma T^4, \\ t_i\dot{a} &= a_{\text{eq}}(T) - a, \\ \frac{M_{CO_2}A}{M_a g}\dot{p}_{CO_2} &= -A_L W + v_{CO_2}. \end{aligned} \tag{2.135}$$

We take $a_{\text{eq}}(T)$ to be given by (2.100), and W to be given by (2.134).

We model the climatic effect of the greenhouse gases CO_2 and H_2O by supposing that γ depends on p_{CO_2}:

$$\gamma = \gamma_0 - \gamma_1 p_{CO_2}; \tag{2.136}$$

the value $\gamma_0 < 1$ represents the H_2O dependence, while the small corrective coefficient γ_1 represents the CO_2 dependence.

We have already seen that the response time of T is rapid, about a month, whereas the time scale for albedo adjustment is slower, with the time scale of growth of continental ice sheets being of order 10^4 years. An estimate for the time scale of adjustment of the atmospheric CO_2, based on this model, is

$$t_c = \frac{M_{CO_2}Ap_0}{M_a g v_{CO_2}}. \tag{2.137}$$

Using values $A = 5.1 \times 10^{14}$ m^2, $p_0 = 36$ Pa, $g = 9.81$ m s^{-2} and $v_{CO_2} = 3.3 \times 10^{11}$ kg y^{-1}, this is $t_c \sim 0.9 \times 10^4$ y, comparable to the ice sheet growth time.

Although (2.135) is a third order system, it is clear that T relaxes rapidly to a well-defined 'slow manifold'

$$T \approx T(a, p_{CO_2}) = \left[\frac{Q(1-a)}{4\sigma\gamma(p_{CO_2})}\right]^{1/4}, \tag{2.138}$$

on which the dynamics are governed by the slower a and p equations. The nullclines in the (a, p) phase plane are shown in Fig. 2.24. The a nullcline is multivalued for

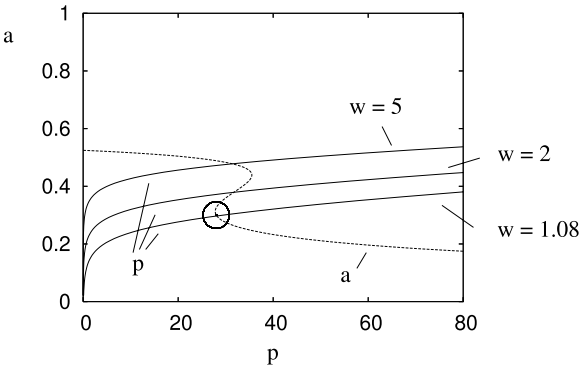

Fig. 2.24 a and p nullclines for (2.135) assuming that T has rapidly equilibrated to $T(a, p_{CO_2})$. The three curves occur for the values of the weathering coefficient $w = 1.08,\ 2$ and 5, corresponding to pre-industrial climate, oscillatory ice ages and snowball Earth. The parameters for a_{eq} are the same as those in Fig. 2.13, and other values used are $p_0 = 36$ Pa, $\mu = 0.3$, $\Delta T_c = 13$ K, $T_0 = 288$ K, $\sigma = 5.67 \times 10^{-8}$ W m^{-2} K^{-4}, $Q = 1370$ W m^{-2}, $\gamma_0 = 0.64$, $\gamma_1 = 0.8 \times 10^{-3}$ Pa^{-1}. The *circle* marks the value $p = 28$ Pa, $a = 0.3$, which corresponds to pre-industrial climate

the same reason that Fig. 2.15 indicates multiplicity, since both graphs are described by the same equations, the only difference being that p_{CO_2} (and thus γ) is used rather than Q. The horizontal axis of Fig. 2.15 could equally be taken to be Q/γ and thus (for fixed Q) p_{CO_2}.

The analysis of this model is indicated in Question 2.16. The solutions depend on the two critical dimensionless parameters

$$w = \frac{A_L W_0}{v_{CO_2}}, \qquad \delta = \frac{v_{CO_2} g t_i M_a}{A p_0 M_{CO_2}}, \tag{2.139}$$

which are measures of weathering rate and volcanic production. These can vary depending on current tectonic style. The three indicated intersection points in Fig. 2.24 correspond to steady states at low (current), intermediate and high weathering rates (relative to volcanic output). The solution on the upper branch indicates a snowball at enhanced weathering rates, as might be expected when the continental land masses are clustered at the equator, promoting tropical climate. Upper and lower branch solutions are stable, but the intermediate solution is oscillatorily unstable if δ is sufficiently small. If δ is very small, then the motion becomes relaxational.

Figure 2.25 shows an oscillatory solution illustrating this discussion. The corresponding time series is shown in Fig. 2.26. It does not look much like the sawtooth oscillation of the Pleistocene ice ages, and the period is too long, some half million years. No doubt one can find something more persuasive by fiddling with parameters, but it is probably not worth the effort, given the enormous simplicity of the model. The main use of the model is to illustrate the point that the carbon cycle contains a feedback effect which is capable of generating self-sustaining oscillations.

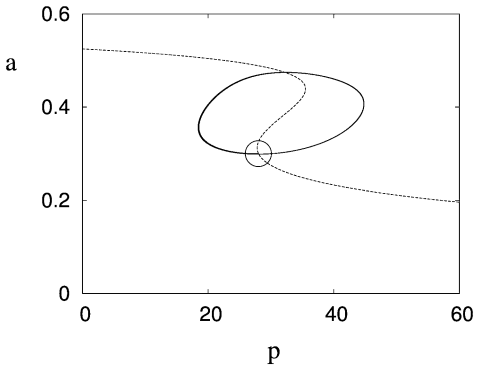

Fig. 2.25 Limit cycle oscillation which passes through pre-industrial climate (indicated by the *circle*) ($T = 288$ K, $a = 0.3$, $p_{CO_2} = 28$ Pa). Also shown is the a nullcline of (2.135). The parameters are those of Fig. 2.24, with $t_i = 10^4$ y, $A = 5.1 \times 10^{14}$ m^2, $A_L = 1.5 \times 10^{14}$ m^2, $g = 9.81$ m s^{-2}. The temperature is taken to be the quasi-equilibrium value of (2.138), and the weathering and eruption rates are taken to be $W_0 = 0.211 \times 10^{-3}$ kg m^{-2} y^{-1}, $v_{CO_2} = 0.15 \times 10^{11}$ kg y^{-1}. With these values, the parameters in (2.139) are $w = 2.11$ and $\delta = 0.0525$. In solving the equations, we take $c = 10^{11}$ J m^{-2} K^{-1}, and thus $\varepsilon = 0.012$, in order to avoid the necessity for impossibly small time steps

Fig. 2.26 Time series of temperature for the periodic oscillation of Fig. 2.25

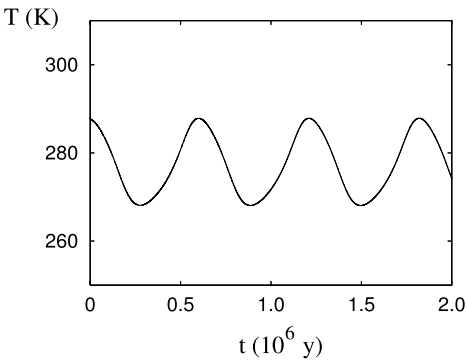

2.6.2 The Rôle of the Oceans

The major simplification which has been made in the above discussion is that we have ignored the part played by the oceans. The oceans hold a good deal more carbon than the atmosphere, although the concentration (as volume fraction) is comparable. They thus act as a buffering mechanism for alterations to atmospheric CO_2.

The oceans also play an important part in another dramatic feature of the Earth's climate, which is indicated by a comparison of the proxy temperature in Fig. 2.12 with a similar graph of atmospheric CO_2 content (see Fig. 2.27). Apart from variations due to noise, the two graphs are essentially the same, which would seem to indicate that ice ages are caused by oscillations in CO_2, since we know that global temperature responds promptly to changes in CO_2. This would be consistent with

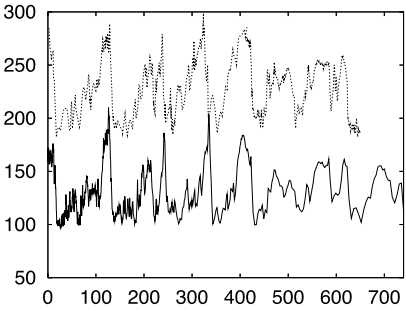

Fig. 2.27 Variation of CO_2 (*upper graph*, units ppmv) with proxy temperature as in Fig. 2.12; horizontal time scale in thousands of years. The deuterium isotope values have been scaled and shifted vertically to point out their resemblance to the CO_2 values

the discussion above. However, temperature also has a direct effect on CO_2, because of respiration of CO_2 by plankton in the oceans, which depends on temperature, and also since the solubility of CO_2 in ocean surface waters depends on temperature; these two facts could then be the mechanism whereby CO_2 conforms with temperature.

A very simple representation of the ocean buffering effect is to add an ocean carbon compartment to the model equations (2.135). Let us denote the concentration of (dissolved inorganic) carbon (not carbon dioxide) in the bulk ocean by C, with units of mol kg^{-1}. This will be different from the surface value, which we denote by C_s, and this difference induces a transport of CO_2 into the ocean proportional to $C_s - C$. To relate this flux to p_{CO_2}, we need to understand the ideas of solubility and of acid–base buffering.

Acid–base buffering, which we analyse further below, describes the partitioning of carbon between dissolved carbon dioxide, bicarbonate, and carbonate ions. Most of the carbon in the oceans resides in the bicarbonate ion reservoir, which is partially maintained by the reaction

$$H_2O + CO_2 \rightleftharpoons HCO_3^- + H^+, \tag{2.140}$$

and from this we find that the CO_2 concentration in the ocean is related to the total dissolved inorganic carbon (DIC) concentration by a partition equation of the form

$$[CO_2] \approx \frac{C}{\left(1 + \frac{K_1}{[H^+]}\right)}, \tag{2.141}$$

where K_1 is the equilibrium constant of (2.140), and [A] denotes the concentration of A.

Next, thermodynamic equilibrium between the CO_2 in the surface waters and the atmosphere is determined by Henry's law, which relates oceanic concentration of CO_2 to the CO_2 partial pressure in the atmosphere. Henry's law takes the form

$$[CO_2]_s = K_H\, p_{CO_2}, \tag{2.142}$$

where the subscript s denotes the ocean surface value. The solubility K_H decreases with increasing temperature, and has units of mol kg^{-1} atm^{-1} (1 atm $= 10^5$ Pa).

Because of the temperature dependence, polar surface waters contain more CO_2 than equatorial waters. The value of K_H in saline oceanic water at 20°C is around 3.5×10^{-2} mol kg^{-1} atm^{-1} (and the value decreases by a factor of about 2.5 between 0°C and 30°C).

With these assumptions, we may take the flux of CO_2 from the atmosphere (in units of kgCO_2 y^{-1}) to be $q = h(p_{CO_2} - \frac{C}{K})$, where

$$K = K_H \left[1 + \frac{K_1}{[H^+]} \right], \tag{2.143}$$

and then the corresponding flux of carbon to the ocean DIC compartment (in mol y^{-1}) is $\frac{q}{M_{CO_2}}$.

In addition, the ocean loses carbon due to the biological pumping effect of carbon uptake by phytoplankton, and its subsequent deposition as organic carbon particles. We take this rate to be bC. The coefficient b will also depend on temperature, and increases with T, due to increased metabolic rates at higher temperatures. A single compartment model for the ocean CO_2 fraction is then

$$\rho_{H_2O} V_{oc} \dot{C} = \frac{1}{M_{CO_2}} \left\{ h \left(p_{CO_2} - \frac{C}{K} \right) + A_L W \right\} - bC, \tag{2.144}$$

where V_{oc} is ocean volume and ρ_{H_2O} is water density. The dynamics of this extended model are the subject of Question 2.17. The essential result is that the atmospheric CO_2 partial pressure follows the ocean DIC concentration, which itself changes on a longer time scale of about 160,000 years. Bistability and even oscillations are still possible, in particular if the biopump coefficient b decreases with increasing ice volume (and thus a). The mechanism whereby this can occur is an interesting one. As ice sheets grow, the continental shelves are exposed, and the biopump effect due to shallow biomass such as coral reefs is removed. It is a noteworthy fact that in the Pleistocene, the ice sheet maximum extent is such that sea level is lower by some 120 m, thus exposing a significant portion of the continental shelves. It is also noteworthy that the snowball Earth class of ice age is associated with pre-Cambrian periods, when hard-shelled creatures did not exist, and the biopump was thus largely absent.

2.6.3 Ocean Acidity

There are a number of chemical constituents of the ocean (most obviously, salt) which affect the acidity of the ocean. But by far the most important of these is the acid–base buffering system of carbon, which is also instrumental in determining the magnitudes of the different carbon reservoirs. In order to determine the partition coefficient in (2.141), it is thus necessary to consider acid–base buffering.

The two principal reactions involve the dissolution of carbon dioxide gas in water to form carbonic acid, which then dissociates to hydrogen ion (acid) H^+ and

bicarbonate ion HCO_3^-. The bicarbonate further dissociates to carbonate ion CO_3^{2-} and acid. The reactions involved are

$$\begin{aligned} H_2O + CO_2 &\underset{k_{-1}}{\overset{k_1}{\rightleftharpoons}} HCO_3^- + H^+, \\ HCO_3^- &\underset{k_{-2}}{\overset{k_2}{\rightleftharpoons}} CO_3^{2-} + H^+, \end{aligned} \tag{2.145}$$

and the corresponding rate equations, based on the law of mass action, are

$$\begin{aligned} [\dot{CO_2}] &= -R_1, \\ [\dot{HCO_3^-}] &= R_1 - R_2, \\ [\dot{H^+}] &= R_1 + R_2, \\ [\dot{CO_3^{2-}}] &= R_2 \end{aligned} \tag{2.146}$$

(we subsume the essentially constant water fraction into the forward rate k_1); square brackets denote concentrations, with units of mol kg^{-1}. The reaction rates are given by

$$\begin{aligned} R_1 &= k_1[CO_2] - k_{-1}[HCO_3^-][H^+], \\ R_2 &= k_2[HCO_3^-] - k_{-2}[CO_3^{2-}][H^+]. \end{aligned} \tag{2.147}$$

These reactions are fast, and equilibrate in a few minutes. Thus we may take $R_1 = R_2 = 0$, whence we find the buffering relationships

$$\begin{aligned} [HCO_3^-][H^+] &= K_1[CO_2], \\ [CO_3^{2-}][H^+] &= K_2[HCO_3^-], \end{aligned} \tag{2.148}$$

where

$$K_1 = \frac{k_1}{k_{-1}}, \qquad K_2 = \frac{k_2}{k_{-2}}. \tag{2.149}$$

Two further relationships are necessary to determine all four concentrations, and these arise from the two independent conservation laws which can be formed from summation of constituents of (2.146). One such is for the total dissolved inorganic carbon (DIC):

$$[CO_2] + [HCO_3^-] + [CO_3^{2-}] = C, \tag{2.150}$$

which we obtain by adding the first, second and fourth of (2.146), and which represents conservation of carbon. In generally, we would also have conservation of oxygen and conservation of hydrogen, but these are not available here since we have not included H_2O as an independent substance. Instead, we can appeal to conservation

of charge, which implies (assuming a zero constant of integration)

$$[HCO_3^-] + 2[CO_3^{2-}] = [H^+], \tag{2.151}$$

and which is evidently an independent conservation law from (2.146).

The conservation of charge equation (2.151) can be used to determine $[H^+]$, wrongly as it will turn out, but the other three equations retain their practical validity when more ionic species are included. In terms of $[H^+]$ we find, using (2.148) and (2.150),

$$[CO_2] = \frac{C}{1 + \frac{K_1}{[H^+]} + \frac{K_1 K_2}{[H^+]^2}}, \tag{2.152}$$

and this is where we obtain (2.143), since the term in K_2 is reasonably small.

We mainly leave it as an exercise to carry through the calculation of $[H^+]$ based on the charge equation (2.151). From (2.148), (2.150) and (2.151), we can derive the cubic equation

$$\xi^3 + \lambda_1 \xi^2 - \lambda_1(1 - \lambda_2)\xi - 2\lambda_1\lambda_2 = 0, \tag{2.153}$$

where

$$\xi = \frac{[H^+]}{C}, \qquad \lambda_1 = \frac{K_1}{C}, \qquad \lambda_2 = \frac{K_2}{C}. \tag{2.154}$$

We use values $C = 2 \times 10^{-3}$ mol kg^{-1}, $K_1 = 1.4 \times 10^{-6}$ mol kg^{-1}, $K_2 = 1.07 \times 10^{-9}$ mol kg^{-1}, and from these we find

$$\lambda_1 \approx 0.7 \times 10^{-3}, \qquad \lambda_2 \approx 0.53 \times 10^{-6}. \tag{2.155}$$

It is easy to show that for positive λ_1 and λ_2, there is precisely one positive solution, and taking $\lambda_2 \sim \lambda_1^2 \ll 1$, this is given approximately by $\xi = \sqrt{\lambda_1}$, and thus

$$[H^+] \approx \sqrt{K_1 C}. \tag{2.156}$$

Using the values given for K_1 and C above, we would compute the pH of seawater to be

$$\text{pH} = -\log_{10}[H^+] \approx 4.28. \tag{2.157}$$

The actual pH of seawater is 8.2, slightly alkaline, whereas this calculation suggests a strongly acid ocean! Thus in using (2.152), we use the actual value of $[H^+] = 0.63 \times 10^{-8}$ mol kg^{-1}. Note that since K_2 is an order of magnitude smaller than this, it is reasonable to neglect the K_2 term in (2.152).

The dynamics of the acid–base buffering system are discussed further in Question 2.18, where the alkalinity of the oceans is indicated as being due to the rôle of calcium carbonate in the carbon buffering system.

2.7 Notes and References

A good, recent book which addresses most of the issues of concern in this chapter is the book by Ruddiman (2001), which provides an expert's view. The book is aimed at undergraduates, and is very accessible. It is only marred by an addiction to design and graphics, which makes the book expensive and rather over the top—it is a book where there is a production team. Despite this, it is very up to date and informative.

Radiative Heat Transfer The classic treatise on radiative heat transfer is the book by Chandrasekhar (1960), although it is dated and not so easy to follow. A more recent book aimed at engineers is that by Sparrow and Cess (1978). Most books on atmospheric physics will have some material on radiative heat transfer, for example those by Houghton (2002) and Andrews (2000). Other books are more specialised, such as those by Liou (2002) and Thomas and Stamnes (1999), but are not necessarily any easier to follow.

Rayleigh scattering is described by Strutt (1871), J. W. Strutt being Lord Rayleigh's given name.

The Ozone Layer The description of the ozone layer dynamics essentially follows Chapman (1930). An elegant exposition is in the book by Andrews (2000). Reality is of course more complicated than the version presented here, and many more reactions can be included, in particular involving catalytic cycles, in which various chemical species catalyse the conversion of ozone to oxygen.

Chlorine species created by man-made chlorofluorocarbons have been implicated in the destruction of stratospheric ozone in the Antarctic, with the formation of the well known 'ozone hole' (Solomon 1999).

Energy Balance Models The original energy-balance models are due to Budyko (1969) and Sellers (1969). They differ essentially only in the choice of parameterisation of emitted long-wave radiation, and consider only the global balance of energy. North (1975a) allows latitude dependent albedo, and additionally allows for a parameterisation of poleward heat transport by oceans and atmosphere through a diffusive term, as in (2.68). North (1975b) added the time derivative. These meridionally averaged energy-balance models do a rather good job of simulating the mean latitude dependent temperature profile, and have formed the basis for the atmospheric component of the more recent models of 'intermediate complexity'. A later review is given by North et al. (1983).

The Greenhouse Effect The first person who is generally credited with discussing the greenhouse effect is Arrhenius (1896), but Arrhenius himself refers to an earlier discussion by Fourier in 1827, where he refers to the atmosphere acting like the glass of a hothouse. Arrhenius's assessments of the effect of CO_2 are rather more severe than today's considered opinion. For a more recent discussion, see Houghton et al. (1996).

Ice Ages The data shown in Figs. 2.17–2.21 are taken from the GRIP (Greenland ice core project) ice core, drilled through the central part of the Greenland ice sheet. These data are provided by the National Snow and Ice Data Centre of the University of Colorado at Boulder, Colorado, and the World Data Centre–A for Paleoclimatology at the National Geophysical Data Centre, also in Boulder, Colorado. This and other such data are publicly available at http://www.ngdc.noaa.gov/paleo/icecore/greenland/summit/index.html and have been reported in a number of publications, for example Johnsen et al. (1992), who, in particular, describe Dansgaard–Oeschger events. The higher resolution data sets in Figs. 2.20 and 2.21 were provided by Sigfus Johnsen, through the agency of Eric Wolff.

Abrupt climate change is documented by Severinghaus and Brook (1999) and Taylor et al. (1997). Taylor et al. (1993) find evidence of rapid ice age climate change in measurements of dust content in ice cores.

The cooling event at 8,200 years B. P. is described by Alley et al. (1997); Leuenberger et al. (1999) calibrate the temperature scale indicated by oxygen isotope variation by studying nitrogen isotope variations, suggesting that the cooling at 8,200 B. P. was of the order of 7 K; see also Lang et al. (1999).

Heinrich Events Heinrich events were first described in North Atlantic deep-sea sediment cores by Heinrich (1988). MacAyeal (1993) introduced his 'binge-purge' model to explain them as a consequence of ice sheet oscillations induced by thermal instability, but assumed that a melting base would automatically cause large ice velocities. Fowler and Schiavi (1998) proposed a more physically realistic model which introduced the concept of hydraulic runaway, and Calov et al. (2002) showed that large scale ice sheets could oscillate somewhat as these earlier studies suggested, using a climate model of 'intermediate complexity' (essentially resolved oceans and ice sheets, and an averaged energy-balance model of atmospheric fluxes).

Dansgaard–Oeschger Events Rahmstorf (2002) gives a nice review of the interplay of oceans and ice sheets in causing climatic oscillations during the last ice age. Ganopolski and Rahmstorf (2001) show how fluctuating freshwater delivery to the North Atlantic can cause abrupt alterations in circulation. The idea that the freshwater pulses might be due to sub-Laurentide jökulhlaups was voiced by Evatt et al. (2006), while similar floods beneath the Antarctic have been described by Goodwin (1988), Wingham et al. (2006) and Fricker et al. (2007).

Oceans and Climate Stommel (1961) introduced the idea of different possible North Atlantic circulations. His model is not too realistic, but nevertheless simple and compelling. Rahmstorf (1995) uses a model of intermediate complexity to examine multiple circulation patterns in the North Atlantic. Depending on the freshwater flux to the North Atlantic, he finds hysteretic switches between different possible flows. Stocker and Johnsen (2003) provide a more recent addition to the subject. Ganopolski and Rahmstorf (2001) provide a convincing picture of how

switches of ocean circulation can cause rapid climate change. Their intermediate complexity model indicates hysteretic switches in ocean circulation due to changes in freshwater flux to the North Atlantic of unknown origin; we have suggested that the origin could be periodic sub-glacial floods. Broecker et al. (1990) and Manabe and Stouffer (1995) provide a similar thesis.

A great advocate of the 1000–2000 year rhythm in climate was Gerard Bond; for example Bond et al. (1999) describe this rhythm, and also suggest that it has continued beyond the end of the ice age (into the Holocene), its most recent manifestation being the little ice age of 1500–1900. See also Bond et al. (1997).

Snowball Earth The idea of a snowball Earth is discussed by Hoffman et al. (1998), for example, although the idea of ancient glaciations had been extant for a long time before that (Harland 1964, 2007). Various modelling efforts have been made to assess the snowball's viability, for example, see Crowley and Baum (1993), Hyde et al. (2000), Chandler and Sohl (2000), and Pierrehumbert (2004).

The Carbon Cycle Our (too) simple model of the interaction of the carbon cycle with ice sheet growth and climate change is based on the discussion of Walker et al. (1981), although their emphasis was on the rôle of CO_2 as a buffer in stabilising climate over geological time, despite the increasing solar luminosity. These ideas are elaborated by Kasting and Ackermann (1986) and Kasting (1989), who consider the effects of very large atmospheric CO_2 concentrations in early Earth history. Kasting (1989) suggests that because of the buffering effect of CO_2, a terrestrial (i.e., with liquid water) planet could be viable out as far as the orbit of Mars. In view of the plentiful evidence of water on Mars in *its* early history, this raises the intriguing prospect of a hysteretic switch from early temperate Mars to present cold Mars.

The buffering effect of CO_2 on climate and the rôle of continental location is discussed by Marshall et al. (1988). Berner et al. (1983) and Lasaga et al. (1985) discuss more complicated chemical models of weathering, and their effect on atmospheric CO_2 levels.

Petit et al. (1999) document the close relation between CO_2 levels and atmospheric temperature over the past 400,000 years, and Agustin et al. (2004) extend this further back in time, as shown in Fig. 2.27. Unlike the result in Fig. 2.25, which together with (2.138), indicates that temperature and CO_2 will vary independently, the data show that there is an excellent match. The model could be made more consistent with this observation if the relaxation time t_i were to be reduced. And indeed, this would not be unreasonable, since the change of albedo due to sea ice coverage will be very fast, and this will shift the effective albedo time scale downwards.

However, it is currently thought that it is the buffering rôle of the oceans which is principally involved in explaining the short term correlation of CO_2 with temperature, and its variation through the ice ages (Toggweiler et al. 2006; Köhler and Fischer 2006). The single compartment model we propose in (2.144) may be the simplest additional complication to add to the basic lumped energy-balance models, but it falls well short of currently fashionable models, which include separate compartments for shallow and deep waters, as well as different compartments for the different oceans (Munhoven and François 1996; Köhler et al.

2005). The apparent necessity for such complexity is to allow a description of the solubility pump (hence the effect of latitude) and the biological pump (hence the effect of depth). The convective interchange between the different compartments occurs on a time scale of several hundred years, consistent with the observation that changes in temperature (at glacial terminations) actually lead the changes of CO_2 by a similar time scale. The surface layers take up CO_2 from the atmosphere, and this is transported to the deep ocean via the global oceanic circulation in the North Atlantic and the Southern Oceans, in particular. Because of the CO_2 solubility dependence on temperature, decreasing temperatures cause an increased flux to the ocean, reducing atmospheric CO_2, and thus providing a positive feedback.

Takahashi et al. (2002) describe the surface flux of CO_2 to the ocean, currently estimated as about 2 PgC y^{-1} (i.e., petagrams, 10^{15} g $= 10^{12}$ kg; 1 kgC corresponds to $10^3/12$ mole C, and if this resides in $10^3/12$ mole CO_2, then this is $44/12 = 3.67$ kg CO_2.

The carbon cycle, and the interchange of CO_2 between ocean and atmosphere, are described in the books by Bigg (2003), Emerson and Hedges (2008) and Krauskopf and Bird (1995). A description together with data on equilibrium constants and solubility is given by Millero (1995). A very useful source is the book by Zeebe and Wolf-Gladrow (2001). While the basic reaction scheme of the carbon buffering system (2.145) is easy enough to understand, it is less easy to get a clear understanding of how the two extra conserved quantities (as for instance (2.150) and (2.151)) should be prescribed. Standard practice (Millero 1995) seems to be simply to measure for example the dissolved inorganic carbon

$$C = [HCO_3^-] + [CO_2] + [CO_3^{2-}], \tag{2.158}$$

and the carbonate alkalinity

$$A = [HCO_3^-] + 2[CO_3^{2-}], \tag{2.159}$$

and from these one can calculate the other concentrations in the system, and thus also the pH. This is the strategy adopted by Emerson and Hedges (2008), and also in Question 2.18. An important addition to the carbon buffering system (2.145) is the dissolution of calcium carbonate, and the total carbon is then determined by this dissolution, as well as by transport from the atmosphere and loss via biological pumping. Charge neutrality does not apply, because of the many other ionic species present. Quite how charge should be determined is not very clear from a theoretical perspective, but the prescription of the (measurable) alkalinity circumvents the necessity of doing this. Krauskopf and Bird (1995, p. 68) do provide a calculation of pH of seawater (they obtain a value of 8.4) based essentially on carbon/calcium conservation (their Eq. (3-11); $P = 0$ in Question 2.18) and on charge neutrality (their Eq. (3-12); $Q = 0$ in Question 2.18). But they also use other observed values, and the calculation is hard to follow. Question 2.18 indicates that these assumptions are not correct, however.[12]

[12]In fact the corrected approach is to assume charge neutrality, but allowing for the net negative charge of the conservative ions: chloride, sodium, etc.

2.8 Exercises

2.1 The planetary albedos of Venus, Mars and Jupiter are 0.77, 0.15, 0.58, respectively, and their distances from the Sun are 0.72, 1.52, 5.20 *astronomical units* (1 a.u. = distance from Earth to the Sun). Calculate the equilibrium temperature of these planets, and compare them with the measured effective black body temperatures, $T_m = 230$ K, 220 K, 130 K. Which, if any, planets appear not to be in equilibrium; can you think why this might be so?

2.2 Show that $\int_{\supset} \cos\theta \, d\omega = \pi$, and deduce that $E_{b\nu} = \pi B_\nu$, where $E_{b\nu}$ is the black body radiation emitted normally from a surface, per unit area.

Use Planck's law

$$B_\nu(T) = \frac{2h\nu^3}{c^2[e^{h\nu/kT} - 1]}$$

to derive the Stefan–Boltzmann law in the form

$$E = \int_0^\infty E_{b\lambda} \, d\lambda = \sigma T^4,$$

where

$$\sigma = \frac{2\pi k^4}{c^2 h^3} \int_0^\infty \frac{z^3 \, dz}{e^z - 1}.$$

By evaluating the integral and using the values $c = 2.998 \times 10^8$ m s^{-1}, $k = 1.381 \times 10^{-23}$ J K^{-1}, $h = 6.626 \times 10^{-34}$ J s, evaluate the Stefan–Boltzmann constant σ.

Hint:

$$\sum_1^\infty \frac{1}{n^4} = \frac{\pi^4}{90}.$$

2.3 In a one-dimensional atmosphere, show that the average intensity is given by

$$J = \frac{1}{2} \int_{-1}^{1} I(\tau, \mu') \, d\mu',$$

and show also that if the energy flux vector is

$$\mathbf{q}_R = \int_{\bigcirc} I(\mathbf{r}, \mathbf{s}) \mathbf{s} \, d\omega(\mathbf{s}),$$

then for a grey atmosphere

$$\nabla . \mathbf{q}_R = -4\pi\kappa\rho[J - B].$$

Deduce that in radiative equilibrium, $J = B$.

2.4 For a purely absorptive atmosphere, show, by interpreting the radiation intensity along a ray path as a probability distribution function for the photon free path length (before absorption), that the mean free path is $1/\rho\kappa_\nu$. Deduce that an optically thin layer is one for which the photon mean free path is larger than the layer thickness.

2.5 In a purely scattering atmosphere, emission occurs by the scattering of radiation in all directions. Suppose that for a beam of intensity I_ν, the loss in intensity in a distance ds due to scattering is $\kappa_\nu I_\nu\, ds$, of which a fraction $P_\nu(\mathbf{s},\mathbf{s}')\, d\omega(\mathbf{s}')/4\pi$ is along a pencil of solid angle $d\omega(\mathbf{s}')$ in the direction $\mathbf{s}'$. Explain why it is reasonable to suppose that the scattering function P_ν should depend only on $\mathbf{s}.\mathbf{s}'$, and show that the equation of radiative transfer can be written (assuming a grey atmosphere)

$$\frac{\partial I}{\partial s} = \rho\kappa\left[-I + \frac{1}{4\pi}\int_{\bigcirc} P(\mathbf{s},\mathbf{s}')I(\mathbf{r},\mathbf{s}')\, d\omega(\mathbf{s}')\right].$$

Deduce that for isotropic scattering, where $P \equiv 1$, the radiative flux $\mathbf{q}_R$ (see Question 2.3) is divergence free.

For a plane parallel atmosphere in which $I = I(\tau,\mu)$, show that

$$\mu\frac{\partial I}{\partial \tau} = I - \frac{1}{4\pi}\int_{-1}^{1}\int_{0}^{2\pi} P(\mathbf{s}.\mathbf{s}')I(\tau,\mu')\, d\mu'\, d\phi',$$

where ϕ' is the azimuthal angle associated with $\mathbf{s}'$. Use spherical polar coordinates to show that

$$\mathbf{s}.\mathbf{s}' = \mu\mu' + \left(1-\mu^2\right)^{1/2}\left(1-\mu'^2\right)^{1/2}\cos(\phi-\phi'),$$

and deduce that for Rayleigh scattering, where $P(\cos\Theta) = \frac{3}{4}(1+\cos^2\Theta)$, I satisfies

$$\mu\frac{\partial I}{\partial \tau} = I - \frac{3}{16}\left[3I_0 - I_2 - \mu^2(I_0 - 3I_2)\right],$$

where $I_0 = \int_{-1}^{1} I\, d\mu$, $I_2 = \int_{-1}^{1}\mu^2 I\, d\mu$.

2.6 By non-dimensionalising the radiative heat transfer equation for a grey atmosphere using a length scale d (atmospheric depth) and an appropriate radiation intensity scale, show that in the optically thick limit, the equation takes the dimensionless form

$$I = B - \varepsilon\, \mathbf{s}.\nabla I,$$

where $\varepsilon \ll 1$ and should be specified. Find an approximate solution to this equation, and hence show that the (dimensional) radiative energy flux vector $\mathbf{q}_R$ is given approximately by

$$\mathbf{q}_R = -\frac{4\sigma}{3\kappa\rho}\nabla T^4.$$

2.7 The equation of radiative transfer in a grey, one-dimensional atmosphere is given by

$$\mu \frac{\partial I}{\partial \tau} = I - B,$$

with $I = 0$ at $\tau = 0$, $\mu < 0$, and $I = B_S \equiv B(\tau_S)$ at $\tau = \tau_S$, $\mu > 0$. Write down the formal solution assuming B is known, and hence show that the radiative flux $q_R = 2\pi \int_{-1}^{1} \mu I \, d\mu$ is given by

$$q_R = 2\pi \Bigg[- \int_0^\tau B(\tau') E_2(\tau - \tau') \, d\tau' + B_S E_3(\tau_S - \tau) + \int_\tau^{\tau_S} B(\tau') E_2(\tau' - \tau) \, d\tau' \Bigg],$$

where the exponential integrals are defined by

$$E_n(z) = \int_1^\infty \frac{e^{-zt} \, dt}{t^n},$$

and $B_S \equiv B(\tau_S)$.

Show that $E_n' = -E_{n-1}$, $E_n(0) = \frac{1}{n-1}$, and deduce that

$$\frac{\partial q_R}{\partial \tau} = 2\pi \Bigg[-2B + B_S E_2(\tau_S - \tau) + \int_0^{\tau_S} B(\tau') E_1\big(|\tau - \tau'|\big) \, d\tau' \Bigg].$$

Show also that the intensity $J = \frac{1}{2} \int_{-1}^{1} I \, d\mu$ is given by

$$J = \frac{1}{2} \Bigg[\int_0^{\tau_S} B(\tau') E_1\big(|\tau - \tau'|\big) \, d\tau' + B_S E_2(\tau_S - \tau) \Bigg].$$

By integrating the expression for q_R by parts, show that

$$q_R = 2\pi \Bigg[B_0 E_3(\tau) + \int_0^{\tau_S} B'(\tau') E_3\big(|\tau - \tau'|\big) \, d\tau' \Bigg]. \qquad (*)$$

If τ_S is large, so that B varies slowly with τ, show that when τ is large,

$$q_R \approx \frac{4\pi}{3} B'(\tau)$$

(essentially, this uses Laplace's method for the asymptotic evaluation of integrals).

Use the integral expression $(*)$ for q_R to show that if $q_R = \pi B_0$ at $\tau = 0$, then

$$\int_0^{\tau_S} B'(\tau') E_3(\tau') \, d\tau' = 0,$$

and deduce that the temperature gradient cannot be monotonic for such an atmosphere.

2.8 Chapman's model for the production of ozone in the stratosphere is

$$\begin{aligned} \mathrm{O}_2 + h\nu &\xrightarrow{j_2} 2\mathrm{O}, \\ \mathrm{O} + \mathrm{O}_2 + \mathrm{M} &\xrightarrow{k_2} \mathrm{O}_3 + \mathrm{M}, \\ \mathrm{O}_3 + h\nu &\xrightarrow{j_3} \mathrm{O} + \mathrm{O}_2, \\ \mathrm{O} + \mathrm{O}_3 &\xrightarrow{k_3} 2\mathrm{O}_2. \end{aligned}$$

Write down the rate equations for the concentrations X, Y and Z of oxygen atoms O, oxygen O_2 and ozone O_3, and show that

$$X + 2Y + 3Z = 2[\mathrm{O}_2],$$

where $[\mathrm{O}_2]$ is constant.

Suppose, as is observed, that $X \ll \frac{j_3}{k_3}$ and $Y \gg \frac{j_3}{k_2[\mathrm{M}]}$, where [M] is the concentration of M. Use these observations to scale the equations to the form

$$\varepsilon \frac{dx}{dt} = z - xy + 2\delta y - \delta xz,$$

$$\frac{dz}{dt} = xy - z - \delta xz,$$

$$y + \frac{1}{2}\lambda(3z + \varepsilon x) = 1,$$

where

$$\varepsilon = \frac{j_3}{k_2[\mathrm{O}_2][\mathrm{M}]}, \qquad \delta = \left[\frac{j_2 k_3}{j_3 k_2[\mathrm{M}]}\right]^{1/2}, \qquad \lambda = \left[\frac{j_2 k_2[\mathrm{M}]}{j_3 k_3}\right]^{1/2}.$$

Assuming $\varepsilon, \delta, \lambda \ll 1$, show that the model can be partially solved to produce the approximate equation

$$\frac{dz}{d\tau} = 2\big(1 - z^2\big),$$

where $t = \tau/\delta$.

Hence show that $[\mathrm{O}_3] \to \lambda[\mathrm{O}_2]$ on a time scale $t \sim (\frac{k_2[\mathrm{M}]}{j_2 j_3 k_3})^{1/2}$, and that the reaction scheme can be represented by the overall reaction

$$3\mathrm{O}_2 \underset{r_-}{\overset{r_+}{\rightleftharpoons}} 2\mathrm{O}_3,$$

where

$$r_+ = \frac{2}{3} j_2, \qquad r_- = \frac{j_3 k_3}{k_2[\mathrm{O}_2][\mathrm{M}]}.$$

2.9 Suppose that stratospheric heating by absorption of ultraviolet radiation is given by

$$Q = -\frac{\partial I}{\partial z},$$

where

$$I = -I_\infty \exp\bigl[-\tau_0 e^{-z/H}\bigr],$$

and

$$\tau_0 = \kappa \rho_0 H, \quad \tau_c = \kappa \rho_c H.$$

Suppose also that the (upwards) long-wave radiative flux is given by

$$q_R = -k_R \frac{\partial T}{\partial z},$$

where the radiative conductivity is given by

$$k_R = \frac{16\sigma T^3 e^{z/H}}{3\kappa \rho_c}.$$

Write down the energy equation describing radiant energy transport, and show that the temperature T is given by

$$T = T_0\bigl[A - \phi e^{-\zeta} - \theta \exp\bigl(-\tau_0 e^{-\zeta}\bigr)\bigr]^{1/4},$$

where A and ϕ are constants, and

$$T_0 = \left(\frac{3I_\infty}{4\sigma}\right)^{1/4}, \qquad \theta = \frac{\tau_c}{\tau_0}, \qquad \zeta = \frac{z}{H}.$$

Suppose that $\phi, \theta, A \sim O(1)$, and that $\tau_0 \gg 1$. Find approximations for T for $\zeta < \ln \tau_0$ and $\zeta \sim \ln \tau_0$, and deduce that T has a maximum at $z \sim H \ln \tau_0$. How is this discussion related to estimation of the temperature in the stratosphere?

2.10 Using values $d = 10$ km, $\kappa \rho d = 0.67$, show that a representative value of the radiative conductivity k_R defined by $\mathbf{q}_R = -k_R \nabla T$ for an opaque atmosphere is $k_R \simeq 1.08 \times 10^5$ W m^{-1} K^{-1}. Hence show that a typical value for the effective Péclet number

$$Pe = \frac{\rho c_p U d^2}{k_R l}$$

is about 20, if $U \approx 20\ \mathrm{m\,s^{-1}}$, $l \approx 1000$ km. Explain the implication of this in terms of the heat equation

$$\rho c_p \frac{dT}{dt} = \nabla.[k_R \nabla T].$$

2.11 A wet adiabat is calculated from the isentropic equation

$$\rho_a c_p \frac{dT}{dz} - \frac{dp}{dz} + \rho_a L \frac{dm}{dz} = 0,$$

where

$$m = \frac{\rho_v}{\rho_a}, \qquad p = \frac{\rho_a RT}{M_a}, \qquad p_{\mathrm{SV}} = \frac{\rho_v RT}{M_v},$$

and

$$\frac{dp_{\mathrm{SV}}}{dT} = \frac{\rho_v L}{T}, \qquad \frac{dp}{dz} = -\rho_a g.$$

Deduce that T and p_{SV} can be calculated from the equations

$$\frac{dT}{dz} = -\Gamma_w(\rho_v, p, T),$$
$$\frac{dp_{\mathrm{SV}}}{dz} = -\frac{\rho_v L}{T}\Gamma_w,$$

where $\rho_v = \rho_v(p_{\mathrm{SV}}, T)$, and Γ_w should be determined. Using values $M_v/M_a = 0.62$, $L = 2.5 \times 10^6\ \mathrm{J\,kg^{-1}}$, $T = 290\ \mathrm{K}$, $c_p = 10^3\ \mathrm{J\,kg^{-1}\,K^{-1}}$, $\rho_v = 0.01\ \mathrm{kg\,m^{-3}}$, $p = 10^5$ Pa, $g = 10\ \mathrm{m\,s^{-2}}$, $\rho_a = 1\ \mathrm{kg\,m^{-3}}$, show that a typical value of Γ_w is $6\ \mathrm{K\,km^{-1}}$.

By assuming that $T \approx$ constant (why?), derive a differential equation for p_{SV} as a function of z in terms of two dimensionless coefficients

$$a = \frac{M_v L}{RT}, \qquad \beta = \frac{M_v}{M_a}\frac{L}{c_p T},$$

and estimate their values (you will need also the values $M_v = 18 \times 10^{-3}\ \mathrm{kg\,mole^{-1}}$, $R = 8.3\ \mathrm{J\,mole^{-1}\,K^{-1}}$). Derive from this an autonomous differential equation for the *molar specific humidity* $h = p_{\mathrm{SV}}/p$. Assuming a surface value of $h \approx 0.02$, show that $H = \beta a h \sim O(1)$, and by writing $z = RTZ/M_a g$ (cf. (2.37)), show that

$$\frac{dH}{dZ} = -\frac{(\beta - 1)H}{1 + H}.$$

Deduce that for $Z \sim O(1)$,

$$H \approx H_0 \exp\big[H_0 - (\beta - 1)Z\big]:$$

humidity decreases rapidly with altitude.

2.12 Show that the solution of the Clausius–Clapeyron equation for saturation vapour pressure p_{SV} as a function of temperature T is

$$p_{SV} = p^0_{SV} \exp\left[a\left\{1 - \frac{T_0}{T}\right\}\right],$$

where for water vapour, we may take $T_0 = 273$ K at $p^0_{SV} = 6$ mbar (= 600 Pa), the *triple point*, and $a = M_v L/RT_0$. Show that if T is close to T_0, then

$$p_{SV} \approx p^0_{SV} \exp\left[a\left(\frac{T - T_0}{T_0}\right)\right].$$

If the long-wave radiation from a planet is $\sigma\gamma T^4$, where T is the mean surface temperature, if the solar flux is Q (and planetary albedo is zero), and the greyness factor is taken to be given by

$$\gamma^{-1/4} = 1 + b\big(p_v/p^0_{SV}\big)^c,$$

where p_v is the H_2O vapour pressure, show that the occurrence of a runaway greenhouse effect is controlled by the intersection of the two curves

$$\theta = 1 + \lambda\xi, \qquad \theta = \rho\big(1 + be^{c\xi}\big),$$

where $\lambda = 1/a$, $\rho = (Q/4\sigma T_0^4)^{1/4}$. Show that runaway occurs if $\rho > \rho_c$, where

$$\rho_c + \delta = 1 + \delta \ln[\delta/b\rho_c]$$

with $\delta = \lambda/c$. Show that this determines a unique value of ρ_c, and that if δ is small,

$$\rho_c \approx 1 + \delta \ln(\delta/b) - \delta.$$

Estimate values of ρ and λ appropriate to the present Earth, and comment on the implications of these values for climatic evolution if we choose $b = 0.06$, $c = 1/4$. What are the implications for Venus, if the solar flux is twice as great? What if solar radiation were 30% lower when the planetary atmospheres were being formed?

2.13 For the energy-balance model

$$c\dot{T} = R_i - R_o,$$

where $R_i = \frac{1}{4}Q(1 - a)$, $R_o = \sigma\gamma T^4$, and $a = a_+$ for $T < T_i$, $a = a_-$ for $T > T_w$ $(> T_i)$, $a_+ > a_-$, with $a(T)$ linear between these two ranges, show that possible steady state values of T are $T = T_i$ when $Q = Q_+$ and $T = T_w$ when $Q = Q_-$, where

$$Q_- = \frac{4\sigma\gamma T_w^4}{1 - a_-}, \qquad Q_+ = \frac{4\sigma\gamma T_i^4}{1 - a_+}.$$

By considering the graphs of R_o and R_i, and the slope of $R_o(T)$ at T_i, show that for Q just less than Q_+, multiple steady states will occur if

$$\frac{T_w - T_i}{T_i} < \frac{a_+ - a_-}{4(1 - a_+)},$$

and in this case show that they will exist in a range $Q_c < Q < Q_+$, and prove that the upper and lower branches are stable, but the intermediate one is unstable.

By considering the slope of $R_o(T)$ at T_w, show that if

$$\frac{T_w - T_i}{T_w} < \frac{a_+ - a_-}{4(1 - a_-)},$$

then $Q_c = Q_-$.

By normalising Q and T with respect to present day values Q_0, T_0 satisfying $Q_0(1 - a_-) = 4\sigma\gamma T_0^4$, show that the corresponding dimensionless solar fluxes and mean atmospheric temperatures, q and θ, satisfy

$$q_- = \theta_w^4,$$
$$q_+ = \theta_i^4\left(\frac{1 - a_-}{1 - a_+}\right),$$

and that multiple steady states will occur providing

$$\frac{\theta_w - \theta_i}{\theta_w} < \frac{a_+ - a_-}{4(1 - a_-)}.$$

If $\theta_w = 1$ (we are starting an ice age *now*) show that if $\theta_i = 1 - \delta$, $a_+ = a_- + \nu$, where $\delta, \nu \ll 1$, then regular ice ages will occur providing

$$\delta < \frac{\nu}{4(1 - a_-)},$$

and providing the solar flux q oscillates beyond the limits

$$q_+ \approx 1 + \frac{\nu}{1 - a_-} - 4\delta$$

and $q_- = 1$.

2.14 Suppose that the planetary albedo a is given by the ordinary differential equation

$$t_i \dot{a} = I(a, Q) - a,$$

where

$$I(a, Q) = a_{\text{eq}}\big[T(a, Q)\big],$$

$$a_{\text{eq}}(T) = a_1 - \frac{1}{2}a_2\left[1 + \tanh\left(\frac{T - T^*}{\Delta T}\right)\right],$$

$$T(a, Q) = \left[\frac{Q(1-a)}{4\sigma\gamma}\right]^{1/4}.$$

Determine the graphical dependence of I as a function of a, and how this varies with Q, and hence describe the form of oscillations if Q is periodic, and t_i is sufficiently small.

For large t_i, show that the equation can be written in the dimensionless form

$$\dot{a} = \varepsilon\big[I\big\{a, Q(t)\big\} - a\big], \qquad (*)$$

where $\varepsilon \ll 1$. The *method of averaging* implies that a varies slowly, and thus can be written approximately as the series

$$a \sim A_0(\tau) + \varepsilon A_1(t, \tau) + \cdots,$$

where $\tau = \varepsilon t$, and

$$\dot{A} = \overline{I(A_0, Q)} - A_0,$$

in which $\overline{I(A_0, Q)}$ denotes the time average of I over a period of Q. Deduce that for a range of values of $\bar{Q}$, two periodic solutions can exist, and comment on their climatic interpretation.

Give explicit approximate solutions of $(*)$ for the cases $\varepsilon \ll 1$ and $\varepsilon \gg 1$ when ΔT is very small.

2.15 Ocean temperature θ and salinity s are described by Stommel's box model

$$\dot{\theta} = 1 - \big(\mu + |\theta - Rs|\big)\theta,$$

$$\dot{s} = \big(1 - |\theta - Rs|\big)s,$$

where μ and R are positive. By analysing the equations in the phase plane, show that up to three steady states can exist, and assess their stability.

By drawing the phase portrait, discuss the nature of the solutions when there is one steady state, and when there are three.

2.16 The temperature T, CO_2 pressure p, and planetary albedo a satisfy the ordinary differential equations

$$c\dot{T} = \frac{1}{4}Q(1-a) - \sigma\gamma T^4,$$

$$t_i\dot{a} = a_{\mathrm{eq}}(T) - a,$$

$$\frac{M_{\mathrm{CO}_2}A}{M_a g}\dot{p} = -A_L W + v,$$

where

$$a_{\mathrm{eq}}(T) = a_1 - \frac{1}{2}a_2\left[1 + \tanh\left(\frac{T - T^*}{\Delta T}\right)\right],$$

where $a_1 = 0.58$, $a_2 = 0.47$, $T^* = 283$ K, $\Delta T = 24$ K,

$$W = W_0\left(\frac{p}{p_0}\right)^{\mu} \exp\left[\frac{T - T_0}{\Delta T_c}\right],$$

and

$$\gamma(p) = \gamma_0 - \gamma_1 p.$$

Show how to non-dimensionalise the system to the dimensionless form

$$\begin{aligned}
\varepsilon\dot{\theta} &= 1 - a - (1 - a_0)\left(1 + \frac{1}{4}\nu\theta\right)^4 (1 - \nu\lambda p),\\
\dot{a} &= B(\theta) - a,\\
\dot{p} &= \alpha\left[1 - wp^{\mu}e^{\theta}\right],
\end{aligned}$$

and show that

$$\alpha = \frac{vgt_i M_a}{Ap_0 M_{\mathrm{CO}_2}}, \qquad w = \frac{A_L W_0}{v}, \qquad \varepsilon = \frac{4c\Delta T_c}{t_i Q},$$
$$\nu = \frac{4\Delta T_c}{T_0}, \qquad \lambda = \frac{\gamma_1 p_0}{\nu\gamma_0}.$$

What is the function $B(\theta)$? What is the definition of a_0?

Using the values $v = 3 \times 10^{11}$ kg y^{-1}, $g = 9.81$ m s^{-2}, $M_a = 28.8 \times 10^{-3}$ kg mole^{-1}, $M_{\mathrm{CO}_2} = 44 \times 10^{-3}$ kg mole^{-1}, $t_i = 10^4$ y, $A = 5.1 \times 10^{14}$ m^2, $p_0 = 36$ Pa, $A_L = 1.5 \times 10^{14}$ m^2, $W_0 = 2 \times 10^{-3}$ kg m^{-2} y^{-1}, $c = 10^7$ J m^{-2} K^{-1}, $Q = 1370$ W m^{-2}, $\Delta T_c = 13$ K, $T_0 = 288$ K, $\gamma_0 = 0.64$, $\gamma_1 = 0.8 \times 10^{-3}$ Pa^{-1}, $\mu = 0.3$, show that

$$\alpha \approx 1.05, \qquad w \approx 1, \qquad \varepsilon \approx 1.2 \times 10^{-6}, \qquad \nu \approx 0.18, \qquad \lambda \approx 0.25,$$

and find the value of a_0, assuming $\sigma = 5.67 \times 10^{-8}$ W m^{-2} K^{-4}.

Hence show that θ rapidly approaches a quasi-steady state given by

$$\theta \approx \Theta(a, p) = \kappa(a_0 - a) + \lambda p,$$

where

$$\kappa = \frac{1}{\nu(1 - a_0)}.$$

In the phase plane of a and p satisfying

$$\begin{aligned}
\dot{a} &= B(\Theta) - a,\\
\dot{p} &= \alpha\left[1 - wp^{\mu}e^{\Theta}\right],
\end{aligned} \qquad (*)$$

show that the p nullcline is a monotonically increasing function $a_p(p)$ of p, and that the a nullcline is a monotonically decreasing function $a_a(p)$ of p,

providing $-B'(\theta) < \nu(1-a_0)$ for all θ. Show conversely that if there is a range of θ for which $-B'(\theta) > \nu(1-a_0)$, then the a nullcline is multivalued.

Suppose that the a nullcline is indeed multivalued, and that there is always a unique steady state. Show that at low, intermediate and high values of w, this equilibrium can lie on the lower, intermediate or upper branch of the a nullcline.

By consideration from the phase plane of the signs of the partial derivatives of the right hand sides of $(*)$ (and without detailed calculation), show that when they exist, the upper and lower branch steady states are stable, but that the intermediate steady state will be oscillatorily unstable if α is small enough.

How would you expect the solutions to behave if $\alpha \ll 1$?

2.17 Suppose now that Question 2.16 is augmented by the addition of a compartment representing ocean carbon storage. Thus we consider the set of equations

$$\begin{aligned} c\dot{T} &= \frac{1}{4}Q(1-a) - \sigma\gamma T^4, \\ t_i\dot{a} &= a_{\mathrm{eq}}(T) - a, \\ \frac{M_{\mathrm{CO_2}}A}{M_a g}\dot{p} &= -A_L W + v - h(p - p_s), \\ \rho_{\mathrm{H_2O}} V_{\mathrm{oc}}\dot{C} &= \frac{h(p-p_s) + A_L W}{M_{\mathrm{CO_2}}} - bC, \end{aligned}$$

where in addition to the variables in Question 2.16, we define the atmospheric partial pressure of CO_2 at the ocean surface to be p_s, and the dissolved inorganic carbon to be C; it is related to the dissolved carbon dioxide $[CO_2]$ by the approximate partitioning relationship

$$C \approx \frac{K_1[\mathrm{CO_2}]}{[\mathrm{H^+}]},$$

where $[H^+] \approx 0.63 \times 10^{-8}$ mol kg^{-1} is the hydrogen ion concentration, and $K_1 \approx 1.4 \times 10^{-6}$ mol kg^{-1} is the equilibrium constant for the dissociation of carbonic acid to bicarbonate and hydrogen ions. $\rho_{\mathrm{H_2O}}$ is the density of seawater, V_{oc} is the volume of the oceans, h is a transport coefficient from atmosphere to the ocean surface, and b is an oceanic biological pump rate coefficient.

Dissolved CO_2 in the ocean is related to the atmospheric surface CO_2 partial pressure p_s by Henry's law,

$$[\mathrm{CO_2}] = K_H p_s.$$

Show how to derive a scaled model in the form

$$\varepsilon\dot{\theta} = 1 - a - (1-a_0)\left(1 + \frac{1}{4}\nu\theta\right)^4 (1 - \nu\lambda p),$$

$$\dot{a} = B(\theta) - a,$$
$$\dot{p} = \alpha\left[1 - wp^{\mu}e^{\theta} - \Lambda\left(p - \frac{C}{s}\right)\right],$$
$$\frac{\beta}{\delta}\dot{C} = p - \frac{C}{s} + \frac{w}{\Lambda}p^{\mu}e^{\theta} - \beta C,$$

where

$$s = \frac{K_H}{K_H^0},$$

and show that the additional parameters (to those in Question 2.16) are defined by

$$\Lambda = \frac{hp_0}{v}, \qquad \beta = \frac{bK_1K_H^0M_{\mathrm{CO}_2}}{h[\mathrm{H}^+]}, \qquad \delta = \frac{bt_i}{\rho_{\mathrm{H}_2\mathrm{O}}V_{\mathrm{oc}}},$$

and that the scale for DIC is

$$C_0 = K_0p_0,$$

where

$$K_0 = \frac{K_1K_H^0}{[\mathrm{H}^+]}.$$

Using the values of Question 2.16, together with a reference value $K_H^0 = 3.465 \times 10^{-2}$ mol kg^{-1} atm^{-1} (and 1 atm $= 10^5$ Pa), $\rho_{\mathrm{H}_2\mathrm{O}} = 1.025 \times 10^3$ kg m^{-3}, $V_{\mathrm{oc}} = 1.35 \times 10^{18}$ m^3, $h = 0.73 \times 10^{17}$ kg y^{-1} atm^{-1} and $b = 0.83 \times 10^{16}$ kg y^{-1}, show that

$$\Lambda \approx 88, \qquad \delta \approx 0.06, \qquad \beta \approx 3.9 \times 10^{-2}.$$

(The values of h and b, and the precise choice of K_H^0, are determined by assuming a biopump flux of 0.2 GtC y^{-1}, current net CO_2 flux to the ocean of 2 GtC y^{-1}, and zero net flux in pre-industrial times; we take $C = 2 \times 10^{-3}$ mol kg^{-1}, $p = 36$ Pa now, and $p = 27$ Pa pre-industrially. These fluxes are those given by Bigg (2003, p. 98); note that 1 GtC $= 10^{12}$ kgC $= 3.67 \times 10^{12}$ kgCO_2, the factor of 3.67 being the ratio of the molecular weights of CO_2 and carbon. The expression K_H given by Emerson and Hedges (2008, p. 98) varies from 7.8×10^{-2} mol kg^{-1} atm^{-1} at 0°C to 3×10^{-2} mol kg^{-1} atm^{-1} at 30°C; the value chosen corresponds to a temperature of 24.25°C. (Note that Emerson and Hedges state that $K_H = 3.24 \times 10^{-2}$ mol kg^{-1} atm^{-1} at 20°C and 35 ppt salinity, whereas the value according to their own tabulated expression would be 3.9×10^{-2}.)

Show that we can take

$$p - \frac{C}{s} + \frac{w}{\Lambda}p^{\mu}e^{\theta} \approx \frac{1}{\Lambda},$$

$$\theta \approx \Theta(a, C) = \frac{\lambda C}{s} + \kappa(a_0 - a)$$

(as in Question 2.16), and deduce that a and C satisfy approximately

$$\dot{a} = B(\Theta) - a,$$

$$\dot{C} = \delta(C^* - C),$$

where $B(\Theta)$ is the same monotonically decreasing function as in Question 2.16, and

$$C^* = \frac{1}{\beta \Lambda} \approx 0.3.$$

Deduce that the ocean carbon relaxes to an equilibrium value over the biopump throughput time scale of $\frac{\rho_{H_2O} V_{oc}}{b} \approx 160$ ky.

Suppose that the biopump transport coefficient varies with a and Θ, thus

$$b = b_0 b^*(a, \Theta).$$

Using b_0 as the scale for b, write down the corresponding model for a and C. How are the dynamics of C affected by the solubility pump and biological pump dependence on Θ (s decreases with Θ and b^* increases with Θ)? If, instead, $s = 1$ and b^* are independent of Θ, what is the effect of b decreasing with a? Can you think of a mechanism why b should have such a dependence?

2.18 Calcium carbonate, $CaCO_3$, in the form of calcite or aragonite, dissolves in acid to form calcium and bicarbonate ions according to the reaction

$$(CaCO_3 +)\ H^+ \underset{k_{-3}}{\overset{k_3}{\rightleftharpoons}} Ca^{2+} + HCO_3^-.$$

In addition, the bicarbonate buffering system is described by the reactions

$$(H_2O +)\ CO_2 \underset{k_{-1}}{\overset{k_1}{\rightleftharpoons}} HCO_3^- + H^+,$$

$$HCO_3^- \underset{k_{-2}}{\overset{k_2}{\rightleftharpoons}} CO_3^{2-} + H^+,$$

where the brackets on H_2O and $CaCO_3$ indicate that these substances are present in unlimited supply, and are thus ignored in writing the rate equations.

Write down the rate equations for the reactant concentrations $[H^+]$, $[Ca^{2+}]$, $[HCO_3^-]$, $[CO_2]$ and $[CO_3^{2-}]$, and by assuming equilibrium, derive three equations for the concentrations in terms of the equilibrium constants

$$K_1 = \frac{k_1}{k_{-1}}, \qquad K_2 = \frac{k_2}{k_{-2}}, \qquad K_3 = \frac{k_3}{k_{-3}},$$

and by suitable summation of the equations, derive the additional relations

$$[\mathrm{HCO_3^-}] - [\mathrm{Ca^{2+}}] + [\mathrm{CO_2}] + [\mathrm{CO_3^{2-}}] = P,$$

$$[\mathrm{H^+}] + 2[\mathrm{Ca^{2+}}] - 2[\mathrm{CO_3^{2-}}] - [\mathrm{HCO_3^-}] = Q,$$

where P and Q are constants.

Define the dissolved inorganic carbon C to be

$$C = [\mathrm{HCO_3^-}] + [\mathrm{CO_2}] + [\mathrm{CO_3^{2-}}],$$

and the alkalinity to be

$$A = [\mathrm{HCO_3^-}] + 2[\mathrm{CO_3^{2-}}].$$

By writing

$$\xi = \frac{[\mathrm{H^+}]}{C}, \qquad \eta = \frac{[\mathrm{CO_2}]}{C}, \qquad p = \frac{[\mathrm{Ca^{2+}}]}{C}, \qquad \lambda_i = \frac{K_i}{C},$$

show that

$$\begin{aligned} \xi + 2p &= q + \alpha, \\ \frac{\lambda_1 \eta}{\xi^2}(\xi + 2\lambda_2) &= \alpha, \\ \frac{\lambda_3 \xi^2}{\lambda_1 \eta} &= p, \\ \eta &= \frac{1}{1 + \frac{\lambda_1}{\xi} + \frac{\lambda_1 \lambda_2}{\xi^2}}, \end{aligned}$$

where

$$P = C(1-p), \qquad Q = Cq, \qquad A = C\alpha.$$

If all the dissolved carbon is formed from calcium carbonate, we may suppose $P = 0$, and if the system is charge neutral, we may take $Q = 0$. Show in this case that ξ satisfies the two equations

$$\xi + 2 = \frac{\lambda_1(\xi + 2\lambda_2)}{\xi^2 + \lambda_1 \xi + \lambda_1 \lambda_2} = \lambda_3(\xi + 2\lambda_2).$$

(*The extra equation occurs because C is not known.*) Show that an exact solution of this pair of equations occurs for $\xi = 0$, $\lambda_2 \lambda_3 = 1$, and deduce that the dissolved carbon concentration is

$$C = \sqrt{K_2 K_3}.$$

Using the values $K_1 = 1.4 \times 10^{-6}$ mol kg^{-1}, $K_2 = 1.07 \times 10^{-9}$ mol kg^{-1} (Emerson and Hedges 2008, p. 105), $K_2K_3 = 1.6 \times 10^{-8}$ mol^2 kg^{-2} (Krauskopf and Bird 1995, p. 76), show that this implies that $C \approx 0.126 \times 10^{-3}$ mol kg^{-1}, which is about sixteen times lower than the observed value. The discrepancy may be ascribed to the presence of many other ionic species, and the presence of other carbonate reactions, so that the assumptions $P = 0$, $Q = 0$ are invalid. Instead we will take the observed values for DIC of $C = 2 \times 10^{-3}$ mol kg^{-1}, and for carbonate alkalinity $A = 2.3 \times 10^{-3}$ mol kg^{-1}. Show in this case that $\alpha = 1.15$, and that

$$\lambda_2 \ll \lambda_1 \ll 1 \ll \lambda_3.$$

By anticipating that $\lambda_2 \lesssim \xi \ll \lambda_1$, show that

$$\xi \approx \left(\frac{2-\alpha}{\alpha-1}\right)\lambda_2, \qquad \eta \approx \frac{(2-\alpha)^2\lambda_2}{(\alpha-1)\lambda_1},$$

and deduce that $\xi \approx 0.3 \times 10^{-5}$, $\eta \approx 0.36 \times 10^{-2}$, and that pH $= -\log_{10}[\mathrm{H}^+] \approx 8.2$, as observed.

Show that the observed concentration of $[\mathrm{Ca}^{2+}] \approx 10^{-2}$ mol kg^{-1} implies that $p \approx 5$, and that then $q \approx 8.85$. Show also that this value of p requires that $\lambda_3 \approx 2.48 \times 10^6$, and thus that $K_2K_3 = 5.3 \times 10^{-6}$ mol^2 kg^{-2}, as opposed to the value quoted above.

2.19 A simple model of the Earth's climate is described by the equations

$$\begin{aligned}
c\dot{T} &= \frac{1}{4}Q(1-a) - \sigma\gamma(p)T^4,\\
t_i\dot{a} &= a_{\mathrm{eq}}(T) - a,\\
\frac{M_{\mathrm{CO_2}}A}{M_a g}\dot{p} &= -A_L W + v - h(p - p_s),\\
\rho_{\mathrm{H_2O}}V_{\mathrm{oc}}\dot{C} &= \frac{h(p-p_s) + A_L W}{M_{\mathrm{CO_2}}} - bC,
\end{aligned}$$

in which T is the absolute temperature of the atmosphere, a is the planetary albedo, p is the mean atmospheric CO_2 partial pressure, p_s is the value of the atmospheric CO_2 partial pressure just above the ocean surface, and C is the dissolved inorganic carbon in the ocean. Explain the meaning of the terms in the equations.

Derive expressions for the relaxation times t_T, t_p and t_C of the T, p and C equations, using the values $a = 0.3$, $T = 288$ K, $Q = 1370$ W m^{-2}, $c = 10^7$ J m^{-2} K^{-1}, $M_{\mathrm{CO_2}} = 44 \times 10^{-3}$ kg mole^{-1}, $A = 5.1 \times 10^{14}$ m^2, $M_a = 28.8 \times 10^{-3}$ kg mole^{-1}, $g = 9.81$ m s^{-2}, $h = 0.73 \times 10^{17}$ kg y^{-1} atm^{-1}, $\rho_{\mathrm{H_2O}} = 1.025 \times 10^3$ kg m^{-3}, $V_{\mathrm{oc}} = 1.35 \times 10^{18}$ m^3 and $b = 0.83 \times 10^{16}$ kg y^{-1}, where also 1 atm $= 10^5$ Pa. Assuming that $t_i = 10^4$ y, show that both T and p rapidly relax to a quasi-steady state, and deduce that a and

C satisfy the approximate pair of equations

$$t_T \dot{a} = B(a, p) - a,$$

$$t_C \dot{C} = C_0 - C.$$

Define C_0, and estimate its value, given that (pre-industrially) $v = 3 \times 10^{11}$ kg y^{-1}. How does this compare with the present day value of $C = 2 \times 10^{-3}$ mol kg^{-1}?

Assuming $p_s = \frac{C}{K}$, where $K = 7.1$ mol kg^{-1} atm^{-1}, and also $A_L = 1.5 \times 10^{14}$ m^2, $W = 2 \times 10^{-3}$ kg m^{-2} y^{-1}, find the pre-industrial value of p (using the present day value of C).

Assuming that current net industrial production of $v_i = 10^{13}$ kg y^{-1} is maintained indefinitely, show that on a time scale of centuries, p will reach an approximate equilibrium, and find its value. Show also that thereafter p will continue to increase more slowly, and sketch the evolution of p with time. What is the eventual value of p?

http://www.springer.com/978-0-85729-699-3

Mathematical Geoscience
Fowler, A.
2011, XIX, 883 p. 211 illus., 6 illus. in color., Hardcover
ISBN: 978-0-85729-699-3